Since January 2020 Elsevier has created a COVID-19 resource centre with free information in English and Mandarin on the novel coronavirus COVID-19. The COVID-19 resource centre is hosted on Elsevier Connect, the company's public news and information website.

Computers in Biology and Medicine 149 (2022) 106046

Contents lists available at ScienceDirect

Computers in Biology and Medicine

journal homepage: www.elsevier.com/locate/compbiomed

SEIR-FMi: A coronavirus disease epidemiological model based on intra-city movement, inter-city movement and medical resource investment

Wen Zhang [a,b,*], Rui Xie [a,b], Xuefan Dong [a,b], Jian Li [a,b], Peng Peng [c], Ernesto DR Santibanez Gonzalez [d]

[a] College of Economics and Management, Beijing University of Technology, Beijing, 100124, PR China
[b] Blockchain Center at Beijing University of Technology, Beijing, 100124, PR China
[c] Beijing Chaoyang Hospital, Beijing, 100150, PR China
[d] Department of Industrial Engineering, Faculty of Engineering, University of Talca, Chile

ARTICLE INFO

Keywords:
COVID-19
SEIR-FMi model
Basic reproduction number
Effective reproduction number
Population movement
Medical resources

ABSTRACT

In this paper, we propose a coronavirus disease (COVID-19) epidemiological model called SEIR-FMi (Susceptible-Exposed-Infectious-Recovery with Flow and Medical investments) to study the effects of intra-city population movement, inter-city population movement, and medical resource investment on the spread of the COVID-19 epidemic. We theoretically derived the reproduction number of the SEIR-FMi model by using the next-generation matrix method and empirically simulate the individual impacts of population movement and medical resource investment on epidemic control. We found that intra- and inter-city population movements will increase the risk of epidemic spread, and the effect of inter-city population movement on low-risk areas is higher than that on high-risk areas. Increasing medical resource investment can not only speed up the recover rate of patients but also reduce the growth rate of infected cases and shorten the spread duration of the epidemic. We collected data on intra-city population movement, inter-city population movement, medical resource investment, and confirmed cases in the cities of Wuhan, Jingzhou, and Xiangyang, Hubei Province, China, from January 15 to March 15, 2020. Using the collected data, we validated that the proposed SEIR-FMi model performs well in simulating the spread of COVID-19 in the three cities. Meanwhile, this study confirms that three non-pharmaceutical interventions, namely community isolation, population mobility control, and medical resource aid, applied during the epidemic period are indispensable in controlling the spread of COVID-19 in the three cities.

1. Introduction

Since late December 2019, the coronavirus disease 2019 (COVID-19) has caused the death of millions of people and brought about a huge economic loss worldwide. During the COVID-19 outbreak, scientific researchers have conducted numerous research studies on the transmission mechanism of the virus [1], and on the prediction, prevention and control of its spread [2–6]. Among these studies, those that developed epidemiological models play an important role in guiding the prevention and control of the COVID-19 epidemic. Although the existing epidemiological models of COVID-19 consider many factors that could affect the spread of the epidemic, some improvements can be made in at least two aspects. First, medical resource investment is usually ignored in these epidemiological models in the current stage. During the epidemic outbreak, investments in medical resources play an important role in patient treatment and epidemic control [7]. Especially in the battle with the COVID-19 outbreak in Wuhan (capital of Hubei province), other provinces in China aided Hubei province with medical resources and staffs, which was recognized by the World Health Organization as one of the successful experiences in response to the outbreak.[1] Thus, medical resource investment must be considered when modeling the spread of COVID-19. Second, the existing studies only considered the impact of population inflow and outflow in a single area [2,3,8], and ignore the impact of population flow between multiple

* Corresponding author. College of Economics and Management, Beijing University of Technology, Beijing, 100124, PR China.
E-mail addresses: zhangwen@bjut.edu.cn (W. Zhang), xierui@emails.bjut.edu.cn (R. Xie), dongxf@bjut.edu.cn (X. Dong), lijiansem@bjut.edu.cn (J. Li), cmupaper@163.com (P. Peng), santibanez.ernesto@gmail.com (E. DR Santibanez Gonzalez).

[1] China's experience needed. Online: https://www.globaltimes.cn/content/1180626.shtml.

https://doi.org/10.1016/j.compbiomed.2022.106046
Received 19 January 2022; Received in revised form 12 August 2022; Accepted 20 August 2022
Available online 31 August 2022

cities. At the same time, little literature has studied the differential impact of population flow for cities with different levels of epidemic development and risk.

On the basis of the classic SEIR (Susceptible-Exposed-Infectious-Recovery) compartmental model, we propose a new epidemiological model called SEIR-FMi (Susceptible-Exposed-Infectious-Recovery with Flow and Medical investments) to study the impact of three factors, namely intra-city population movement, inter-city population movement, and medical resource investment, on the spread of the COVID-19 epidemic by model simulation. Using the next-generation matrix method, we derived the basic reproduction number and effective reproduction number of the proposed SEIR-FMi model and theoretically demonstrated the impact of intra-city population movement, inter-city population movement, and medical resource investment on the spread of the epidemic. Finally, we used the proposed model to simulate the spread of the COVID-19 epidemic in three cities in Hubei Province, namely Wuhan, Jingzhou, and Xiangyang, from January 24, 2020, to March 15, 2020. By comparing the real results with the simulation outcomes, we demonstrate that non-pharmaceutical interventions such as community isolation, population mobility control, and medical resource aid implemented in Hubei Province in this period exerted an indefensible effect on controlling the spread of COVID-19 in the three cities. Moreover, we find that low-risk cities are more vulnerable to the effects of population flow than high-risk cities.

2. Literature review

2.1. Epidemiological models

Viral transmission in the population is a complex diffusion process. Thus, scientific researchers are striving to discover the viral propagation mechanism in terms of mathematical analysis and simulation models [9,10]. The current epidemiological models can be roughly classified into three categories: cellular automata-based epidemiological model [11,12], agent-based epidemiological model [13–15], and epidemiological compartment model [23].

Cellular automaton (CA) is a simulation model of a complex dynamical system in a discrete finite-state cell space according to local rules. It consists of four components of a cellular space (C): a finite-state set of all cells (Q), a finite set of indexes adjacent to each cell (V), and a set of rules for cell change (F). CA can be used to describe complex systems consisting of the interactions of multiple individuals in a regular space and is often used to model the spread of infectious diseases in complex situations. For instance, Bouaine et al. [12] used CA to study the effect of population migration and climate change on the spread of infectious diseases. Sirakoulis et al. [16] used CA to study the effects of population movement and the presence of immune groups on the spread of infectious diseases. Moreover, we also notice that the network modeling [17,18] is introduced to model the complex dynamic system with the goal to study the impact of network structure on the spread of infectious diseases [19–22].

The agent-based epidemiological model is an extension of CA that can simulate human activities and describe complex spatial environments with geographic information. For this reason, it can reflect the epidemic spread in more detail. Silva et al. [13] studied the development of the COVID-19 epidemic under different social distancing intervention schemes (including conditional lockdown, quarantine, and use of face masks) based on the agent-based model. They reported that partial quarantine and mask wearing are the most effective strategies when considering socioeconomics. Cliff et al. [14] proposed an agent-based epidemiological model with 19.8 million agents to simulate the dynamics of disease spread at multiple sites in Australia. They reported that their model can reproduce the epidemic propagation process with high accuracy.

The SIR model proposed by Kermack et al., in 1927 [23] is widely accepted in the research area as a classic epidemiological compartment model. This model classifies the population into three different compartments: susceptible, infected, and recovered. On the basis of the classic SIR model, researchers can improve the compartment model in two ways. First, researchers can extend the classic compartment model to deal with different scenarios in real practice. For instance, the SEIR model extends the SIR model by adding the exposed compartment considering the disease incubation period [5,6]. The SEQIR model extends the SIR model by adding the quarantined compartment considering isolation measures [24,25]. The SEIAR model extends the SIR model by adding the asymptomatic infected compartment considering the presence of asymptomatic infected during an infectious disease [8]. Second, researchers consider more factors that would influence the epidemic spread on the basis of the classic SIR model. For instance, the epidemiological model with an age structure considers the age characteristics of susceptible people [26,27]. The epidemiological patch model considers the migration of individuals between different groups [28,29]. The limited medical resource model considers the impact of medical resource on the cure rate of the disease [7,29].

2.2. SEIR model

The classic SEIR model is widely used to model the spread dynamics of COVID-19 because the model considers the incubation period of the epidemic [6,35,36]. In the SEIR model, the whole population is divided into one of the following four states: susceptible (S, denotes the set of persons who are not yet infected but are at risk of being infectious), exposed (E, denotes the set of persons who are already infected but not showing symptoms), infectious (I, denotes the set of exposed persons who developed symptoms after the incubation period or confirmed as infected by medical testing), and recovered (R, denotes the set of persons who have recovered from the epidemic). Furthermore, the SEIR model for COVID-19 is built with the following hypotheses:

(H-1): Recovered individuals are given a long period of immunity after having developed antibodies; thus, they will not become susceptible again in the model.

(H-2): In some of the early studies on the SEIR model [32,33], researchers assumed that the exposed persons consists of individuals that are infected by virus but not infectious. However, unlike the existing studies, the patients infected with COVID-19 virus can infect others in the incubation period [6,8]. Therefore, many epidemiological models of the COVID-19 assumed that exposed individuals can infect susceptible ones [8,30]. In this paper, we also assume that the exposed individuals can infect susceptible individual before the onset of symptom.

(H-3): The effects of natural birth and death rates on the epidemic spread are not considered in the model.

The model is given by the following ordinary differential equation system. All the other parameters are summarized in Table 1.

$$\begin{cases} \dfrac{\mathrm{dS}}{dt} = -\left[q\left(\dfrac{I}{N}\right) + p\left(\dfrac{E}{N}\right)\right]\mathrm{S} \\ \dfrac{d\mathrm{E}}{dt} = \left[q\left(\dfrac{I}{N}\right) + p\left(\dfrac{E}{N}\right)\right]\mathrm{S} - \varepsilon E \\ \dfrac{dI}{dt} = \varepsilon E - \gamma I \\ \dfrac{dR}{dt} = \gamma I \end{cases} \tag{1}$$

Table 1
Definitions of the parameters in the SEIR model.

Parameter	Description
N	Total population, $N = S + E + I + R$
p	Effective infection rate between the susceptible and the infected
q	Effective infection rate between the susceptible and the exposed
ε	Transfer rate from exposed to infected
γ	Recovery rate of the infected

In the SEIR model, at each time step (in days in later analyses), susceptible individuals would be exposed with probability q or p if they have contact with an infected individual or an exposed individual. An individual exposed with an infected individual would become infected with probability ε after an incubation period. An infected individual would recover with probability γ.

2.3. Population mobility and spread of the epidemic

Recently, the development of transportation worldwide has greatly changed the travel patterns of people and made epidemic spread easier than before because of the fast population mobility across different regions. For some cities with large populations and developed infrastructures and transportation networks, both inward and outward epidemic spread are highly possible [29]. For instance, severe acute respiratory syndrome (SARS) and COVID-19 infections spread from densely populated and developed transportation cities to surrounding cities [26]. Thus, it is important to understand the epidemic spread from the perspective of population mobility patterns [3,34]. Accordingly, Hanski proposed the meta-population theory to divide populations into subpopulations with spatial structures according to geographic location [35]. Gatto et al. [36] studied the impact of population movement on viral transmission from macroscopic and microscopic aspects.

On the macroscopic aspect, Wang et al. [28] proposed a patch (i.e., subpopulation) model that assumes that the viral transmission within each patch follows the SIR compartment model and assumes heterogeneous migration rates of population movement between the patches. Ruan et al. [29] proposed a multi-regional model to study the spread of the SARS virus in different geographic areas. They reported that the return rate of people in a region has a significant effect on the number of infected and the basic reproduction number in the region.

On the microscopic aspect, researchers use big data on mobile communication and global flight to build a spatial network model of population movement to study the impact of population mobility on viral transmission [2,36]. Chang et al. [2] used cell phone location data to obtain population movement information for 10 cities in the United States and construct a people travel network. On the basis of this network, they found that restaurants and places of worship are the main areas that caused the spread of the virus. Although the spatial network model is mathematically complete in characterizing people contact and disease transmission, the primary mechanism behind node generation and edge linking in modeling the real epidemic spread is still unclear. Moreover, its high computational volume has limited value for real infectious disease prevention and control [37].

2.4. Medical resource and epidemic spread

In the classic epidemiological models, the recovery rate of the infected individual is usually set as a constant. However, in real practice, most epidemics tend to produce a larger number of infected individuals in a short time. This outcome will cause an insufficient supply of medical resources and lower the recovery rate of patients. Thus, Many scholars suggest that the recovery rate is nonlinearly dependent on the number of patients and resources available to the medical system [38]. Wang [39] proposed a segmented linear recovery rate function (see Eq. (2)) that shows that when the number of patients I is small and the medical resources r are uniformly distributed, the recovery rate $T(I)$ is proportional to the medical resources and the number of patients. However, when the number of patients is larger than the threshold I_0, the recovery rate $T(I)$ is a constant m.

$$T(I)=\begin{cases} Ir & 0 \le I \le I_0 \\ m & I > I_0 \end{cases} \tag{2}$$

Zhang et al. [40] proposed a continuous and unsaturated recovery rate function (see Eq. (3)), here r denotes the medical resource and a denotes the delayed recovery rate. When the number of patients I is small, the recovery rate $\mathrm{T}(I)$ positively correlated with the medical resource $r(\mathrm{T}(I) \approx rI)$. When the number of patients I is large, the recovery rate is fixed $(\mathrm{T}(I) \approx r/a)$.

$$\mathrm{T}(I)=\frac{rI}{1+aI} \tag{3}$$

Many medical resource factors determine the recovery rate, such as the number of health-care workers, including physicians, nurses, and pharmacists, and the number of hospital facilities, including beds and medicines. Among these factors, the number of hospital beds is widely used by health planners as a method of estimating resource availability to the public. Shan et al. [38] proposed a dynamic recovery rate function (see Eq. (4)) based on the numbers of beds and patients, here $\gamma_{\max}$ denotes the maximum recovery rate at the time of maximum number of beds, $\gamma_{\min}$ denotes the minimum recovery rate at the time of shortage of beds, and $b(t)$ denotes the total number of beds at the time t.

$$T[b(t),I]=\gamma_{\min}+(\gamma_{\max}-\gamma_{\min})\frac{b(t)}{b(t)+I} \tag{4}$$

Eq. (4) shows that when the number of infected patients is small or the number of beds is large enough, the recovery rate of patients $T[b(t),I]$ will be high. However, when the number of patients I is much larger than the number of beds $b(t)$, the recovery rate $T[b(t),I]$ will be low. This is in line with the actual medical resources needed for patient treatment. Thus, the function in Eq. (4) is widely adopted in the current infectious disease model [7,41]. For this reason, we also adopt the dynamic recovery rate function in our proposed SEIR-FMi model.

3. Proposed SEIR-FMi model

3.1. Mathematical model of SEIR-FMi

Our proposed SEIR-FMi model improves the classical SEIR model in three aspects. First, we considered the impact of intra-city population movement on the spread of the COVID-19 epidemic and introduced the intra-city movement intensity variable a in the SEIR-FMi model. The intra-city movement intensity is exponential to the ratio of the mobility population to the living population in a city. We use it to measure the level of people's mobility and contact activity within the city. The population activity intensity directly influences the infection probability of the susceptible population. A high intra-city movement intensity indicates that the susceptible population has a high probability of contracting the virus.

Second, when studying the epidemic spread in a city, the population inflow from other cities, especially from the city of epidemic foci, must be considered. Considering that the infected and recovered are quarantined during the COVID-19 epidemic outbreak, we assume that these people do not move between cities, and only the susceptible and exposed move between cities. Meanwhile, the exposed will spread the virus to the target city and infect the susceptible during the movement. Therefore, we introduce three aspects into the SEIR-FMi model: the inflow and outflow of susceptible and exposed populations between cities and the occurrence of infection in population movement.

Finally, considering the influence of medical resource investment on the epidemic, we adopted the dynamic recovery rate function (see Eq. (4)) proposed by Shan [38]. First, compared with other models, Eq. (4) puts forward the maximum and minimum recovery rates, which can more truly reflect the recovery rate under different medical resources and the number of infected people, and we can use the maximum and minimum recovery rates to measure the goodness of the model. Second, compared with other factors of medical resource, the number of hospital beds can be a good indicator of the level of medical resource in a region and is easier to obtain. Therefore, according to Eq. (4), we used the number of hospital beds in each city over time to denote the level of medical resources and define the recovery rate as a function of the

numbers of beds and current infections.

Combining the above three factors, we propose the SEIR-FMi epidemiological model as shown in Eq. (5). All the parameters of the proposed SEIR-FMi model are summarized in Table 2.

$$\begin{cases} \dfrac{dS_i}{dt} = -\left[a_i p_i\left(\dfrac{I_i}{N_i}\right) + a_i q_i\left(\dfrac{E_i}{N_i}\right)\right]S_i - \sum\limits_{j=1,j\neq i}^{m} \dfrac{a_i q_i E_j S_i}{N_i}\left(\dfrac{F_{j,i}}{S_j+E_j}\right) + \sum\limits_{j=1,j\neq i}^{m}\left(\dfrac{F_{j,i}}{S_j+E_j}\right)S_j - \sum\limits_{j=1,j\neq i}^{m}\left(\dfrac{F_{i,j}}{S_i+E_i}\right)S_i \\ \dfrac{dE_i}{dt} = \left[a_i p_i\left(\dfrac{I_i}{N_i}\right) + a_i q_i\left(\dfrac{E_i}{N_i}\right)\right]S_i + \sum\limits_{j=1,j\neq i}^{m} \dfrac{a_i q_i E_j S_i}{N_i}\left(\dfrac{F_{j,i}}{S_j+E_j}\right) + \sum\limits_{j=1,j\neq i}^{m}\left(\dfrac{F_{j,i}}{S_j+E_j}\right)E_j - \sum\limits_{j=1,j\neq i}^{m}\left(\dfrac{F_{i,j}}{S_i+E_i}\right)E_i - \varepsilon_i E_i \\ \dfrac{dI_i}{dt} = \varepsilon_i E_i - \gamma_i[b_i(t), I_i]I_i, \quad \gamma_i[b_i(t), I_i] = \gamma_{\min} + (\gamma_{\max} - \gamma_{\min})\dfrac{b_i(t)}{b_i(t)+I_i} \\ \dfrac{dR_i}{dt} = \gamma_i[b_i(t), I_i]I_i \end{cases} \tag{5}$$

The flow diagram of the proposed SEIR-FMi model is shown in Fig. 1. At each time step t, a susceptible individual S_i in city i will be infected by an infected individual I_i or an exposed individualE_i with the given probabilities. The parameter p_i denotes the probability that a susceptible individual is infected by an infected individual in the same city. The parameter q_i denotes the probability that a susceptible individual is infected by an exposed individual in the same city. During the incubation period, an exposed individual will be diagnosed as infected with the probability ε_i. Eventually, this infected individual will recover with the probability $\gamma_i[b_i(t),\ I_i]$. Meanwhile, the susceptible population $\sum_{j=1,j\neq i}^{m}\left(\frac{F_{j,i}}{S_j+E_j}\right)S_j$ and exposed population $\sum_{j=1,j\neq i}^{m}\left(\frac{F_{j,i}}{S_j+E_j}\right)E_j$ in other cities move to city i. The susceptible population $\sum_{j=1,j\neq i}^{m}\left(\frac{F_{i,j}}{S_i+E_i}\right)S_i$ and exposed population $\sum_{j=1,j\neq i}^{m}\left(\frac{F_{i,j}}{S_i+E_i}\right)E_i$ in city i move to other cities. This will influence the numbers of people in the S, E, I, and R compartments among all the cities.

3.2. Reproduction number calculation of the SEIR-FMi model

The basic reproduction number R_0 can be defined as the number of new infections produced by an infected individual during the entire infectious period [42], which reflects the transmission ability of a virus during the early stage of an outbreak [43]. However, as the epidemic spreads, the social situation is changing with the implementation of control measures, such as reduced population movement and increased medical resources. Therefore, with the change of social situation, the basic reproduction number is no longer a fixed constant but a time-varying variable [49]. Considering the change of the actual social situation, we use the effective reproduction number $R_e(t)$ to denote the time-varying transmission ability of virus, which means the number of secondary cases that an infected individual could bring about at time t when all the other conditions are remained the same. By using the next-generation matrix approach [42,49], we derive the basic reproduction number R_0 and the effective reproduction number $R_e(t)$ of the proposed SEIR-FMi model.

We assume that the initial condition $S_i(0) + E_i(0) + I_i(0) + R_i(0) \geq 0$, $N_i(0) = N^*$ at time $t = 0$, which indicates that the total population of city i at the initial time is N^*. Let the compartment vector $X = (x_E, x_I, x_S, x_R)^T$, here x_E, x_I, x_S, and x_R denote the number of persons in the exposed, infected, susceptible, and recovered compartments, respectively. It is easy to check that the disease-free equilibrium is given by the point at $X^* = (0, 0, N^*, 0)$.

Let $J(x) = (J_E(x), J_I(x), J_S(x), J_R(x))^T$ be the generation rate of the newly infected individuals in each compartment and $V(x) = (V_E(x), V_I(x), V_S(x), V_R(x))^T$ be the transfer rate of individual movement in each compartment. Based on the proposed SEIR-FMi model, we can derive $J(x)$ and $V(x)$ as follows:

$$J(x) = \begin{pmatrix} \left[a_i p_i\left(\dfrac{I_i}{N_i}\right) + a_i q_i\left(\dfrac{E_i}{N_i}\right)\right]S_i + \sum\limits_{j=1,j\neq i}^{m} \dfrac{a_i q_i E_j S_i}{N_i}\left(\dfrac{F_{j,i}}{S_j+E_j}\right) \\ 0 \\ 0 \\ 0 \end{pmatrix} \tag{6}$$

$$V(x) = \begin{pmatrix} -\sum\limits_{j=1,j\neq i}^{m}\left(\dfrac{F_{j,i}}{S_j+E_j}\right)E_j + \sum\limits_{j=1,j\neq i}^{m}\left(\dfrac{F_{i,j}}{S_i+E_i}\right)E_i + \varepsilon_i E_i \\ -\varepsilon_i E_i + \gamma_i[b_i(t), I_i]I_i \\ \left[a_i p_i\left(\dfrac{I_i}{N_i}\right) + a_i q_i\left(\dfrac{E_i}{N_i}\right)\right]S_i + \sum\limits_{j=1,j\neq i}^{m} \dfrac{a_i q_i E_j S_i}{N_i}\left(\dfrac{F_{j,i}}{S_j+E_j}\right) - \sum\limits_{j=1,j\neq i}^{m}\left(\dfrac{S_j F_{j,i}}{S_j+E_j}\right) + \sum\limits_{j=1,j\neq i}^{m}\left(\dfrac{S_i F_{i,j}}{S_i+E_i}\right) \\ -\gamma_i[b_i(t), I_i]I_i \end{pmatrix} \tag{7}$$

We define $DJ(x)$ and $DV(x)$ as the Jacobian matrices of $J(x)$ and $V(x)$, respectively. Then, we can obtain the Jacobian matrices $DJ|_{X=X^*} = \begin{pmatrix} \mathbf{F} & 0 \\ 0 & 0 \end{pmatrix}$ and $DV|_{X=X^*} = \begin{pmatrix} \mathbf{V} & 0 \\ \mathbf{J}_1 & \mathbf{J}_2 \end{pmatrix}$ at the disease-free equilibrium point X^*, here $\mathbf{F}$ and $\mathbf{V}$ denote the infection and transfer force matrices for the population in the diseased individual compartment. Furthermore, we

Table 2
Definitions of the parameters of the SEIR-FMi model.

Parameters	Description
i	The i th city in the model, $i \in [0,m]$
S_i	Number of susceptible in the city i
E_i	Number of exposed in the city i
I_i	Number of infected in the city i
R_i	Number of recovered in the city i
N_i	Total population in the city i, $N_i = +S_i + E_i + I_i + R_i$
a_i	Intra-city movement intensity of the city i
p_i	Effective infection rate between the susceptible and infected in the city i
q_i	Effective infection rate between the susceptible and the exposed in the city i
$F_{j,i}$	Number of people moving from city j to city i
ε_i	Transfer rate from exposed to infected in the city i
γ_{max}	Maximum recovery rate
γ_{min}	Minimum recovery rate
$b_i(t)$	Total number of beds in the city i at time t

obtain $\mathbf{F} = \begin{pmatrix} F_{11} & F_{12} \\ 0 & 0 \end{pmatrix}$, $\mathbf{V} = \begin{pmatrix} V_{11} & 0 \\ V_{21} & V_{22} \end{pmatrix}$, here $F_{11} = diag(a_1q_1, a_2q_2, ..., a_mq_m)(\mathbf{D}_m + \mathbf{M})$, $F_{12} = diag(a_1p_1, a_2p_2, ..., a_mp_m)$, $V_{11} = diag(\varepsilon_1, \varepsilon_2, ..., \varepsilon_m)(\mathbf{D}_m + \mathbf{M})$, $V_{21} = -diag(\varepsilon_1, \varepsilon_2, ..., \varepsilon_m)$, $V_{22} = diag(\gamma_1', \gamma_2', ..., \gamma_m')$ and $\gamma_i' = \gamma_{min} + (\gamma_{max} - \gamma_{min})\left[\frac{b_i(t)}{b_i(t)+I_i(t)}\right]^2$. $\mathbf{D}_m$ denotes an $m \times m$ identity matrix, $\mathbf{M} = \{m_{ij}\}(i,j \in [0,m])$ denotes the flow rate matrices of the populations of city j to city i, and $diag()$ is a diagonal matrix. According to the next-generation matrix approach [42,49], the basic reproduction number for the proposed SEIR-FMi model is the spectral radius of the next-generation matrix $\mathbf{FV}^{-1}$. Therefore, the basic reproduction number for all cities as a whole R_0 based on the proposed SEIR-FMi model as follow.

$$R_0 = \rho(\mathbf{FV}^{-1}) = \rho\left(\begin{pmatrix} F_{11} & F_{12} \\ 0 & 0 \end{pmatrix}\begin{pmatrix} V_{11}^{-1} & 0 \\ V_{22}^{-1}V_{21}V_{11}^{-1} & V_{22}^{-1} \end{pmatrix}\right) := \rho(F_{11}V_{11}^{-1} + F_{12}V_{22}^{-1}V_{21}V_{11}^{-1}) \tag{8}$$

For simplicity, we take two cities (cities A and B) as the examples and derive the whole basic reproduction number for two cities. We assume that the intra-city movement intensity and the number of inter-city population movements are all the same as that of the initial condition of the COVID-19 epidemic. For computational convenience, let $\lambda_1 = F_{1,2}/(E_1 + S_1)$ be the proportion of the number of people moving from city A to city B to the total number of susceptible and exposed in city A at the beginning of epidemic. Let $\lambda_2 = F_{2,1}/(S_2 + E_2)$ be the proportion of the number of people moving from city B to city A to the total number of susceptible and exposed in city B at the beginning of epidemic. Because the number of infections at the beginning of the epidemic is equal to 0, the recovery rates for both cities A and B are the maximum as $\gamma_1 = \gamma_2 = \gamma_{max}$. Thus, the proposed SEIR-FMi model can be described in Eq. (9).

$$\begin{cases} \frac{dS_1}{dt} = -a_1\left(p_1\left(\frac{I_1}{N_1}\right) + q_1\left(\frac{E_1}{N_1}\right)\right)S_1 - a_1q_1\frac{\lambda_2E_2}{N_1}S_1 + \lambda_2S_2 - \lambda_1S_1 \\ \frac{dS_2}{dt} = -a_2\left(p_2\left(\frac{I_2}{N_2}\right) + q_2\left(\frac{E_2}{N_2}\right)\right)S_2 - a_2q_2\frac{\lambda_1E_1}{N_2}S_2 + \lambda_1S_1 - \lambda_2S_2 \\ \frac{dE_1}{dt} = a_1\left(p_1\left(\frac{I_1}{N_1}\right) + q_1\left(\frac{E_1}{N_1}\right)\right)S_1 + a_1q_1\frac{\lambda_2E_2}{N_1}S_1 + \lambda_2E_2 - \lambda_1E_1 - \varepsilon_1E_1 \\ \frac{dE_2}{dt} = a_2\left(p_2\left(\frac{I_2}{N_2}\right) + q_2\left(\frac{E_2}{N_2}\right)\right)S_2 + a_2q_2\frac{\lambda_1E_1}{N_1}S_1 + \lambda_1E_1 - \lambda_2E_2 - \varepsilon_2E_2 \\ \frac{dI_1}{dt} = \varepsilon_1E_1 - \gamma_1I_1; \quad \frac{dI_2}{dt} = \varepsilon_2E_2 - \gamma_2I_2; \quad \frac{dR_1}{dt} = \gamma_1I_1; \quad \frac{dR_2}{dt} = \gamma_2I_2 \end{cases} \tag{9}$$

With Eq. (9), the infection and transfer force matrices can be derived as Eqs. (10) and (11), respectively.

$$\mathbf{F} = \begin{bmatrix} a_1q_1 & a_1q_1\lambda_2 & a_1p_1 & 0 \\ a_2q_2\lambda_1 & a_2q_2 & 0 & a_2p_2 \\ 0 & 0 & 0 & 0 \\ 0 & 0 & 0 & 0 \end{bmatrix} \tag{10}$$

$$\mathbf{V} = \begin{bmatrix} \lambda_1 + \varepsilon_1 & -\lambda_2 & 0 & 0 \\ -\lambda_1 & \lambda_2 + \varepsilon_2 & 0 & 0 \\ -\varepsilon_1 & 0 & \gamma_1 & 0 \\ 0 & -\varepsilon_2 & 0 & \gamma_2 \end{bmatrix} \tag{11}$$

To simplify the calculation, we assume that the transfer rates from exposed to infected in the two cities are equivalent (i.e., $\varepsilon_1 = \varepsilon_2 = \varepsilon$). Based on the next-generation matrix method, the whole basic reproduction number of city A and B can be derived in Eq. (12).

$$R_0 = \rho(\mathbf{FV}^{-1}) \approx \frac{a_1p_1}{2\gamma_1} + \frac{a_2p_2}{2\gamma_2} + \frac{a_1q_1 + a_2q_2}{2\varepsilon} + \frac{a_1q_1\lambda_2 + a_2q_2\lambda_1}{2\varepsilon} \tag{12}$$

Considering the changes of population movements and medical resources with the implement of control measures, the reproduction number is no longer a constant. Thus, we use the effective reproduction number $R_e(t)$ to reflect the time-varying transmission ability of virus. We set the$a_i(t)$ as intra-city movement intensity of the city$i$ at time$t$, $F_{i,j}(t)$ as number of people moving from city$j$ to city$i$ at time$t$, and $\gamma_i(t) = \gamma_{min} + (\gamma_{max} - \gamma_{min})\frac{b_i(t)}{b_i(t)+I_i(t)}$ as the dynamic recovery rate of city i at time$t$. By analogy, for computational convenience, let $\lambda_1(t) = F_{1,2}(t)/(E_1 + S_1)$ be the proportion of the number of people

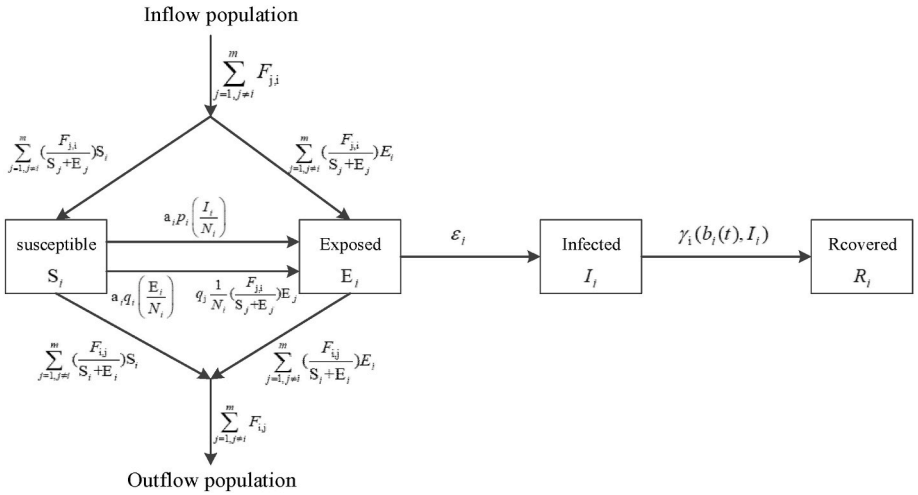

Fig. 1. Flow diagram of the SEIR-FMi model.

moving from city A to city B to the total number of susceptible and exposed in city A at time t. Let $\lambda_2(t) = F_{2,1}(t)/(S_2 + E_2)$ be the proportion of the number of people moving from city B to city A to the total number of susceptible and exposed in city B at time t. Similarly, we can derive the infection and transfer force matrices as Eqs (13) and (14), respectively.

$$\mathbf{F} = \begin{bmatrix} a_1(t)q_1 & a_1(t)q_1\lambda_2(t) & a_1(t)p_1 & 0 \\ a_2(t)q_2\lambda_1(t) & a_2(t)q_2 & 0 & a_2(t)p_2 \\ 0 & 0 & 0 & 0 \\ 0 & 0 & 0 & 0 \end{bmatrix} \tag{13}$$

$$\mathbf{V} = \begin{bmatrix} \lambda_1(t) + \varepsilon_1 & -\lambda_2(t) & 0 & 0 \\ -\lambda_1(t) & \lambda_2(t) + \varepsilon_2 & 0 & 0 \\ -\varepsilon_1 & 0 & \gamma_1'(t) & 0 \\ 0 & -\varepsilon_2 & 0 & \gamma_2'(t) \end{bmatrix} \tag{14}$$

Here, the $\gamma_1'(t) = \gamma_{\min} + (\gamma_{\max} - \gamma_{\min})\left[\frac{b_1(t)}{b_1(t)+I_1(t)}\right]^2$ and $\gamma_2'(t) = \gamma_{\min} + (\gamma_{\max} - \gamma_{\min})\left[\frac{b_2(t)}{b_2(t)+I_2(t)}\right]^2$. We assume that the transfer rates from exposed to infected in the two cities are equivalent (i.e., $\varepsilon_1 = \varepsilon_2 = \varepsilon$). Based on the next-generation matrix method, the whole effective reproduction number of city A and B is derived as shown in Eq. (15).

$$R_e(t) = \rho\left(\mathbf{F}\mathbf{V}^{-1}\right) \approx \frac{a_1(t)p_1}{2\gamma_1'(t)} + \frac{a_2(t)p_2}{2\gamma_2'(t)} + \frac{a_1(t)q_1 + a_2(t)q_2}{2\varepsilon} + \frac{a_1(t)q_1\lambda_2(t) + a_2(t)q_2\lambda_1(t)}{2\varepsilon} \tag{15}$$

By deducing the partial derivative of effective reproduction number $R_e(t)$ on intra-city movement intensity, we can obtain $\frac{\partial R_e(t)}{\partial a_1(t)} = \frac{p_1}{2\gamma_1'(t)} + \frac{q_1[1+\lambda_2(t)]}{2\varepsilon} > 0$ and $\frac{\partial R_e(t)}{\partial a_2(t)} = \frac{p_2}{2\gamma_2'(t)} + \frac{q_2[1+\lambda_1(t)]}{2\varepsilon} > 0$, which indicates that the intra-city movement intensities $a_1(t)$ and $a_2(t)$ positively affects the effective reproduction number. Therefore, during the spread of the epidemic, the denser the intra-city population movement, the higher the number of infections in both cities. Similarly, we can derive $\frac{\partial R_e(t)}{\partial \lambda_1(t)} = \frac{a_2(t)q_2}{2\varepsilon} > 0$ and $\frac{\partial R_e(t)}{\partial \lambda_2(t)} = \frac{a_1(t)q_1}{2\varepsilon} > 0$, which indicates that the inter-city population movement proportion $\lambda_1(t)$ and $\lambda_2(t)$ also positively affects the effective reproduction number. The increases in the numbers of moving population between two cities as $F_{1,2}(t)$ and$F_{2,1}(t)$ will increase the inter-city population movement proportions as$\lambda_1(t) = F_{1,2}(t)/(E_1 + S_1)$ and $\lambda_2(t) = F_{2,1}(t)/(S_2 + E_2)$. Consequently, it will also increase the effective reproduction number. Therefore, during the spread of the epidemic, a large population flow between cities will lead to a serious epidemic development. In addition, we can obtain partial derivatives as $\frac{\partial R_e(t)}{\partial \gamma_1'(t)} = -\frac{a_1(t)p_1}{2(\gamma_1'(t))^2} < 0$, $\frac{\partial R_e(t)}{\partial \gamma_2'(t)} = -\frac{a_2(t)p_2}{2(\gamma_2'(t))^2} < 0$, which indicates that the larger the health-care resource investment, the higher the dynamic recovery rates $\gamma_1'(t)$ and $\gamma_2'(t)$, and thus the lower the effective reproduction number of the disease. Therefore, during the epidemic spread, enough medical resource investment for tackling the epidemic will mitigate the epidemic spread in the city.

Furthermore, we give the effective reproduction number for city i based on the proposed model (see Eq. (5)). In this case, we assume that the epidemic trends in other cities is not influenced by city i. Therefore, the proportion of susceptible and exposed individuals in the population of other cities will not influenced by city i. For simplicity, let $\lambda_{i,j}(t) = F_{i,j}(t)/(E_i + S_i)$ be the proportion of the outflow population from city$i$ to city j to the total number of susceptible and exposed in city$i$ at time$t$, and $\lambda_{j,i}(t) = F_{j,i}(t)/(E_j + S_j)$ be the proportion of the inflow population from city j to city i to the total number of susceptible and exposed in city j at time t. Based on Eq. (5), the infection and transfer force matrices of city i can be derived as Eqs. (16) and (17), respectively.

$$\mathbf{F} = \begin{bmatrix} a_i(t)q_i & a_i(t)p_i \\ 0 & 0 \end{bmatrix} \tag{16}$$

$$\mathbf{V} = \begin{bmatrix} \sum_{j=1,j\neq i}^{m} \lambda_{i,j}(t) + \varepsilon_i & 0 \\ -\varepsilon_i & \gamma_i'(t) \end{bmatrix} \tag{17}$$

Based on the next-generation matrix method, the effective reproduction number for city i is derived as shown in Eq. (18).

$$R_e^i(t) = \frac{a_i(t)q_i}{\sum_{j=1,j\neq i}^{m} \lambda_{i,j}(t) + \varepsilon_i} + \frac{a_i(t)p_i\varepsilon_i}{\gamma_i'(t)\left[\sum_{j=1,j\neq i}^{m} \lambda_{i,j}(t) + \varepsilon_i\right]} \tag{18}$$

Eq. (18) shows that the effective reproduction number $R_e^i(t)$ for city i is positively affected by intra-city movement intensity $a_i(t)$ and negatively affected by medical source investment $\gamma_i'(t)$. Moreover, the more people are exported from the city i (i.e., $\sum_{j=1,j\neq i}^{m}\lambda_{i,j}(t)$), the smaller the effective reproduction number $R_e^i(t)$.

4. Model simulation

4.1. Data collection

We selected three cities, namely Wuhan, Jingzhou, and Xiangyang, in Hubei Province, China, to examine the appropriateness of the proposed SEIR-FMi model by conducting simulation experiments. We investigated the impact of the epidemic prevention and control measures on the development of the COVID-19 epidemic. In December 2019, the outbreak of the COVID-19 epidemic began in Wuhan. Wuhan City is one of the transportation hubs in China, where a larger number of people travel between Wuhan and other cities. In addition, two cities, Jingzhou and Xiangyang, were selected for analysis in this study. These cities have similar resident populations and have large population flow (in and out) between Wuhan. The three cities have obvious geographical boundaries to differentiate them and have large-population movements in the usual time. This elaborates our observation on the collected data of population movement.

The data used in our study can be divided into three parts. The first is the actual infected cases data of COVID-19 in the three cities. We collected the actual infected case data of the COVID-19 epidemic from the official websites of Hubei Provincial Health Committee, which include the number of new infection cases, the total number of infections cases, and the number of new cured cases per day in the three cities from January 15 to May 20, 2020.

The second is the data on intra- and inter-city population movements across the three cities. We collected the population movement data from the Baidu Migration Big Data Platform, which includes the population movement data of the three cities for each day from January 15 to March 15, 2020. Baidu Migration Big Data Platform is an open data platform (online: https://qianxi.baidu.com/#/2020chunyun). That platform records the population migration data based on city size during 2020 spring festival in China. The source of the data in this platform is from user location services embedded in the Apps provided by Baidu such as Baidu Map, Baidu News and Baidu Search. Because Baidu Apps have a large number of users and a great market share in China, the Baidu Migration Big Data Platform can provide us with an approximately accurate population travel data [44]. The data in this platform is open and free to use and we collect the data used in our paper by network crawler. Although there might be a small difference between the data provided by this platform and the real numbers of population migration, we regard that it can reflect an overall status of the actual population travel during 2020 spring festival in China. There are also some existing studies [44,45] that also use the data from this platform to study the population movement and COVID-19 in China.

The third is the data of the total number of hospital beds in each city during the COVID-19 epidemic. We collected the bed data of the designated and square cabin hospitals from the official websites of the

Table 3
Real data information.

Data description	Source	Period	Minimum	Maximum
Number of infected with COVID-19 in Wuhan	Hubei province Health Committee	2020/1/15–2020/5/20	227	37925
Number of infected with COVID-19 in Xiangyang		2020/1/15–2020/5/20	1	1025
Number of infected with COVID-19 in Jingzhou		2020/1/15–2020/5/20	1	1241
Intensity of intra-city population movement in Wuhan	Baidu migrates big data platform	2020/1/15–2020/3/15	0.56	5.33
Intensity of intra-city population movement in Jingzhou		2020/1/15–2020/3/15	1.49	6.21
Intensity of intra-city population movement in Xiangyang		2020/1/15–2020/3/15	1.27	6.2
Number of migrant population: Wuhan > Xiangyang		2020/1/15–2020/3/15	202	19181
Number of migrant population: Wuhan > Jingzhou		2020/1/15–2020/3/15	272	22644
Number of migrant population: Jingzhou > Wuhan		2020/1/15–2020/3/15	777	7584
Number of migrant population: Jingzhou > Xiangyang		2020/1/15–2020/3/15	80	932
Number of migrant population: Xiangyang > Wuhan		2020/1/15–2020/3/15	424	4531
Number of migrant population: Xiangyang > Jingzhou		2020/1/15–2020/3/15	50	1007
Number of hospital beds in Wuhan	Health Committee of Wuhan[a]	2020/1/15–2020/3/15	600	60500
Number of hospital beds in Xiangyang	Health Committee of Xiangyang[b]	2020/1/15–2020/3/15	100	5367
Number of hospital beds in Jingzhou	Health Committee of Jingzhou[c]	2020/1/15–2020/3/15	100	4508

[a] Health Committee of Wuhan. Online: http://wjw.wuhan.gov.cn/.
[b] Health Committee of Xiangyang. Online: http://wjw.xiangyang.gov.cn/.
[c] Health Committee of Jingzhou. Online: http://wjw.jingzhou.gov.cn/.

health committees of the three cities. Table 3 shows the information on the detailed data sources.

Fig. 2 shows the daily intra-city population movement intensities in Wuhan, Jingzhou, and Xiangyang from January 15, 2020, to May 20, 2020. From January 1 (New Year's Day) to January 23, 2020 (Chinese New Year's Eve), the intra-city population movement intensity gradually increased. On January 24, 2020, the Hubei province activated the level I public health emergency response to the Wuhan COVID-19 epidemic outbreak. Thereafter, the intra-city population movement intensities in the three cities rapidly decreased.

Fig. 3 shows the inter-city movements in the three cities from January 15 to March 15, 2020. The inter-city movement between the three cities is at a high level until January 24, 2020. Most people moved

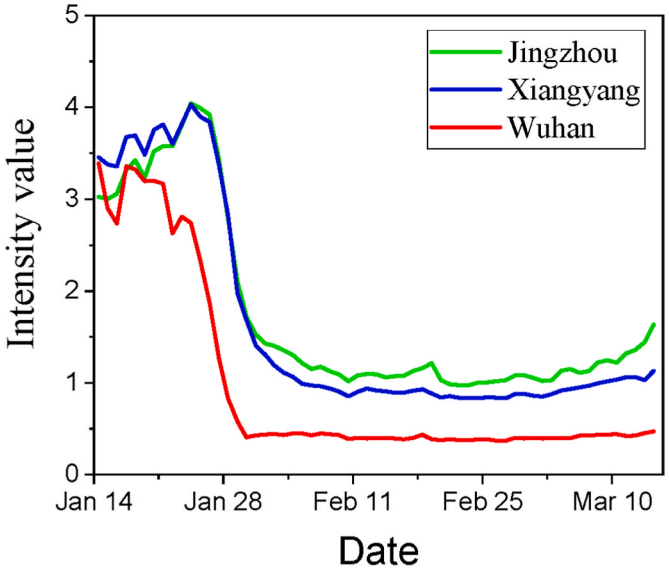

Fig. 2. Intra-city population movement of Wuhan, Jingzhou and Xiangyang.

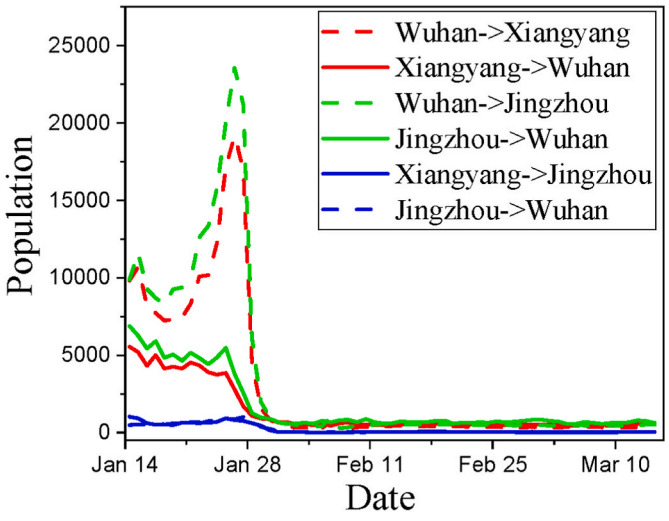

Fig. 3. Inter-city population movements between Wuhan, Jingzhou, and Xiangyang.

out from Wuhan to Jingzhou and Xiangyang because many Wuhan residents returned to their homes to celebrate the Chinese Spring Festival. After January 24, the inter-city movement rapidly decreased owing to the level I public health emergency response and the lockdown of Wuhan.

Fig. 4 shows the numbers of hospital beds in the three cities. The hospital bed capacities in Jingzhou and Xiangyang increased rapidly from February 7, 2020, because medical resource aids were initiated on February 7 by the joint prevention and control mechanism of the State Council. Medical resources from outside provinces gradually entered the Hubei province after February 11, 2020. In Wuhan, the number of hospital beds started to increase on January 25 and peaked on February 28 as the square-cabin hospitals in the city started to provide beds for patients. After March 7, the number of beds began to decline because the epidemic in Wuhan was controlled; thus, the officials decided to stop the construction of more square-cabin hospitals.

4.2. Parameter estimation

Before using the SEIR-FMi model, the model parameters, including

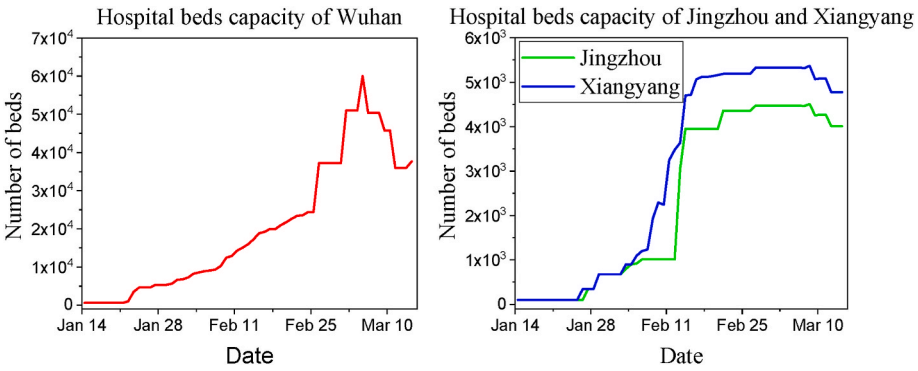

Fig. 4. Hospital bed capacities in Wuhan, Jingzhou, and Xiangyang.

Table 4
SEIR-FMi model parameters.

Parameters	Wuhan		Jingzhou		Xiangyang	
	Values	95% CIs	Values	95% CIs	Values	95% CIs
p	0.301	(0.296, 0.306)	0.265	(0.260, 0.270)	0.265	(0.260, 0.270)
q	0.001	(0.0008,0.0012)	0.0013	(0.0011,0.0015)	0.0012	(0.0001,0.0014)
ε	0.153	(0.149, 0.157)	0.12	(0.116, 0.124)	0.1303	(0.126, 0.134)
$\gamma_{\min}$	0.05	(0.055, 0.045)	0.05	(0.055, 0.045)	0.05	(0.055, 0.045)
$\gamma_{\max}$	0.14	(0.137, 0.143)	0.14	(0.137, 0.143)	0.14	(0.137, 0.143)

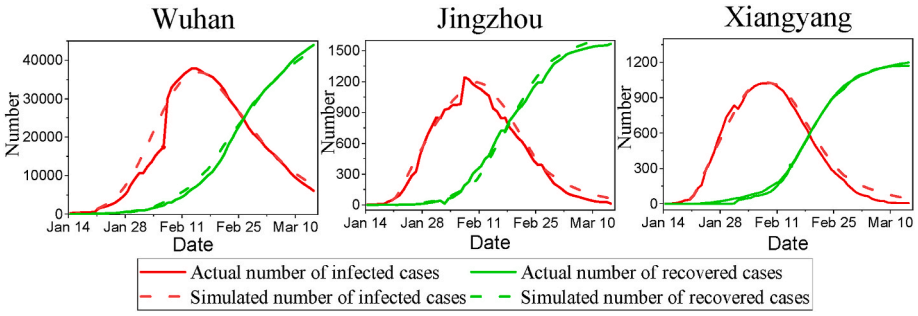

Fig. 5. Real epidemic and the simulated spread by the proposed SEIR-FMi model.

the infection rates p and q, the transfer rate from exposed to infected ε, and the maximum recovery rate $\gamma_{\max}$ and minimum recovery rate $\gamma_{\min}$, must be estimated for each city. By using real epidemic data from January 20, 2020 to March 15, 2020, we fitted the proposed SEIR-FMi model and derived the estimates of the parameters. Specifically, we adopt a two-step parameter estimation method in this paper [46,47]. Firstly, we estimate a set of outcomes by minimizing the Sum of Squared Errors (SSE) of total number of infected cases between the model simulation outcomes and actual epidemic data. The SSE function is minimized with the gradient-based method by setting the iteration number as 10 000 [47]. Secondly, we use the estimated set of parameters as the initial values of the Markov Chain Monte Carlo (MCMC) approach [48]. Similar to the approach used by Zu et al. [46], we set the iteration number to 8000 and the first 6000 iterations as burn-in periods. Finally, we obtain the estimated parameters in proposed SEIR-FMi model. In Table 4, we list the estimated values of parameters, as well as its corresponding 95% confidence intervals (CIs).

Table 4 shows that the transfer rates (i.e., ε) from exposed to infected were 0.153, 0.12, and 0.1303 in Wuhan, Jingzhou, and Xiangyang, respectively. The reciprocal values of the three transfer rates ranged from 6 to 8, which is consistent with the 6- to 8-day average incubation period given by the World Health Organization for COVID-19 [24]. The maximum and minimum recovery rates were 0.14 and 0.05, respectively, in all three cities. The reciprocal values of the two recovery rates ranged from 7 to 20, which are also consistent with the average cure period range given by the World Health Organization for patients with COVID-19 [31]. On the basis of the results of the parameter estimates, the proposed SEIR-FMi model performs better in characterizing the real epidemic spread than the traditional SEIR model.

Fig. 5 shows the number of infected cases fitted using the SEIR-FMi model and the number of infected cases in the three cities. The model fitting results are close to the real results on the infected and recovered curves, which indicates that the proposed SEIR-FMi model is good at fitting the real epidemic spread in the three cities.

4.3. Calculate the effective reproduction number

Based on Eq. (15) and Eq. (18), we calculate the time-varying effective reproduction number $R_e(t)$ for Wuhan, Jingzhou and Xiangyang as a whole and for each of the city. Moreover, we calculate the effective reproduction number R_e^i for each of city under the best situation and the worst situation.

Firstly, we give the whole effective reproduction numbers of three cities over time under the actual situation in Fig. 6. We can see that at the beginning of the COVID-19 outbreak, the whole $R_e(t)$ for the three cities was about 5.5. From about January 25th, $R_e(t)$ quickly dropped to nearly 1. By around March 20, $R_e(t)$ gradually dropped to below 1, indicating that the COVID-19 is under control at this time. For each of

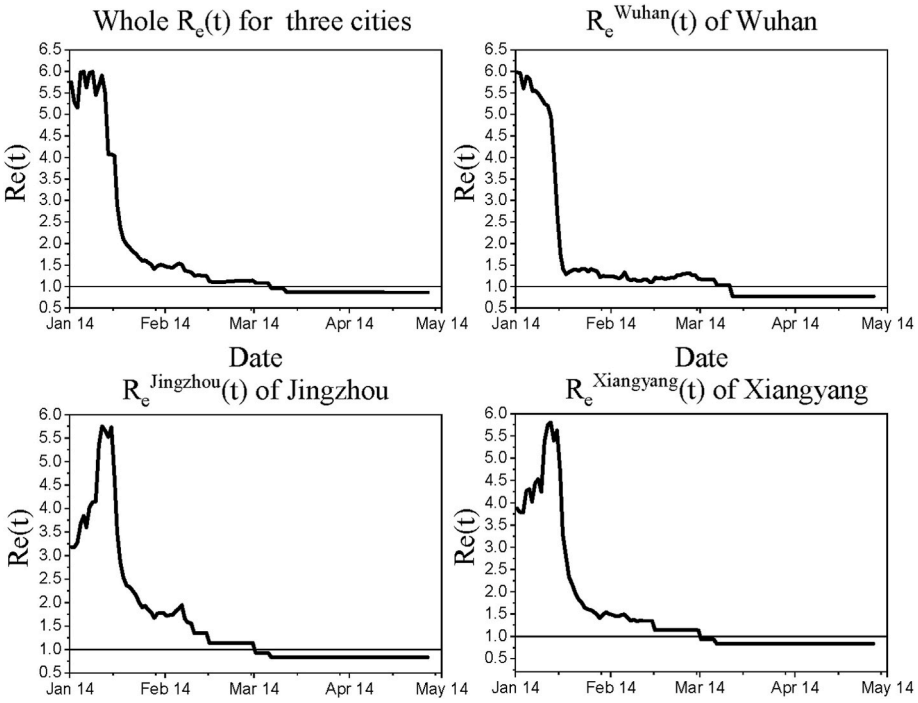

Fig. 6. The effective reproduction number for three cities as a whole and for each city under actual situation.

Table 5
Effective reproduction number of Wuhan, Jingzhou and Xiangyang under the best and worst situation.

Situation	$R_e^{Wuhan}(t)$ for Wuhan	$R_e^{Jingzhou}(t)$ for Jingzhou	$R_e^{Xiangyang}(t)$ for Xiangyang	$R_e(t)$ for three cities as a whole
Best	0.777	0.703	0.703	1.036
Worst	6.261	5.938	5.938	6.045

the city, the effective reproduction number of the Wuhan $R_e^{Wuhan}(t)$ was about 5.9 at the beginning of the COVID-19 outbreak, but quickly dropped to near 1 at middle of February. Until mid-March, its effective reproduction number gradually dropped to below 1. The effective reproduction number of Jingzhou $R_e^{Jingzhou}(t)$ and the effective reproduction number Xiangyang $R_e^{Xiangyang}(t)$ from January 15th to 25th were gradually increased, because the intra-city movement intensity $a_i(t)$ for the two cities were increased and the number of hospital beds $b_i(t)$ were not increased during this time. Until the level I public health emergency response was implemented on January 24, 2020, the effective reproduction number of Jingzhou and Xiangyang were gradually decreased to near 1. Around March 14, both Jingzhou's effective reproduction number $R_e^{Jingzhou}(t)$ and Xiangyang's effective reproduction number $R_e^{Xiangyang}(t)$ dropped to below 1. Thus, we can find that all the three cities have a relatively high effective reproduction numbers at the early stage of the COVID-19 outbreak. With the implementation of population movement control measures and medical investment measures on January 24, 2020, the effective reproduction number began to decrease. In the late March 2020, the epidemic gradually receded.

Furthermore, we calculate the effective reproduction number for a single city under the best situation and the worst situation. According to Equation (18), we can see that for a single city, its effective reproduction number $R_e^i(t)$ can be reduced by reducing its intra-city population movement intensity $a_i(t)$, increasing its medical resources investment $\gamma_i'(t)$, and increasing its city population outflow $\sum_{j=1,j\neq i}^{m}\lambda_{ij}(t)$. Therefore, the best situation for a single city is to have the lowest intra-city movement intensity, the largest number of hospital beds and the largest outflow population. On the contrary, the worst situation for a single city is to have the highest intra-city movement intensity, the least number of hospital beds and the least out-flow population. We also calculate the effective reproduction number $R_e(t)$ for three cities as a whole when all of them are in the best and worst situations separately.

Table 6
Experiment scenarios design.

Scenario	Community isolation measure	Inter-city mobility control measure	Medical resource aid measure
1	No	Yes	Yes
2	7 days delayed	Yes	Yes
3	7 days early	Yes	Yes
4	Yes	No	Yes
5	Yes	7 days delayed	Yes
6	Yes	7 days early	Yes
7	Yes	Yes	No
8	Yes	Yes	7 days delayed
9	Yes	Yes	7 days early

Table 5 shows the effective reproduction number of the three cities under the best and worst situations. The effective reproduction number for each city under the best situation is smaller than 1, which means that if a city is considered individually, the epidemic can be eliminated by restricting travel within the city, increasing medical investment, and increasing the outflow population. However, when all the cities are at its best situation, the effective reproduction number $R_e(t)$ for the three cities as a whole is greater than 1. The reason lies in two sides. On the one side, it is impossible that all the three cities are at its best situations at the same time on the condition that the epidemic is spreading. On the other side, although the effective reproduction number for an individual city can be reduced by increasing outflow population (see Eq. (18)), the outflow population also increase the epidemic risk of other cities. Thus, when a city increases its outflow population to reduce its effective reproduction number, it would increase the whole $R_e(t)$ for the three cities as a whole (see Eq. (15)). Therefore, it is unadvisable to increase the outflow population if a city has developed the epidemic, because this will increase the epidemic risks of other cities as well as the epidemic

risk of all the cities as a whole. The effective reproduction number for each city and for all the cities as a whole are nearly 6 under the worst situation, which means that without the control measures, the epidemic can spread quickly in cities and cause large numbers of infected persons.

4.4. Simulation scenario setup

With the fitted SEIR-FMi model, we simulate the COVID-19 epidemic spread in the three cities by counterfactual analysis. The Level I public health emergency response includes community isolation, inter-city population mobility control and medical resource aid that exactly corresponds to the measures on intra-city population movement, inter-city population movement, and medical resources investment. Following the line of Ye [15] and Ge [49], we also set the impact of different timing of the implementation of the Level I public health emergency response as one week earlier or one week later. Thus, we setup 9 scenarios in Table 6 to study the effects of intra-city population movement, inter-city population movement, and medical resources aid on the COVID-19 spread.

We design scenarios 1 to 3 to study the impact of intra-city movement on the spread of COVID-19. In the three scenarios, the three cities of Wuhan, Jingzhou, and Xiangyang were assume to maintain inter-city population mobility control and medical resource aid during the COVID-19 epidemic outbreak. In scenario 1, community isolation was not implemented on January 24, 2020, and the population movement intensities in the three cities were kept at the same levels as those before January 24, 2020. In scenario 2, community isolation was implemented 7 days later, while the population movement intensities in the three cities remained at the same levels as those before January 24 until January 31, 2020, and were controlled and thus decreased after January 31, 2020. In scenario 3, community isolation was implemented 7 days earlier, while the population movement intensities in the three cities were at the same levels as those before January 17, 2020, and were controlled and thus decreased after January 17, 2020.

We designed scenarios 4 to 6 to study the impact of inter-city movement on the spread of COVID-19. In the three scenarios, we assumed that the three cities of Wuhan, Jingzhou, and Xiangyang maintained community isolation and medical resource aid during the COVID-19 epidemic outbreak. In scenario 4, inter-city mobility control was not implemented on January 24, 2020, and the number of mobile populations between the three cities remained at the same level as that in 2019. In scenario 5, inter-city mobility control was implemented 7 days later, while the population mobility between the three cities remained at the same level as that in 2019 until January 31, 2020, and was controlled and thus decreased rapidly after January 31, 2020. In scenario 6, inter-city mobility control was implemented 7 days earlier, while the population movement between the three cities before January 17, 2020, remained at the same level as that in 2019 and was controlled and thus decreased after January 17, 2020.

We designed scenarios 7 to 9 to study the impact of medical resource aid on the spread of COVID-19. In the three scenarios, we assumed that the three cities of Wuhan, Jingzhou, and Xiangyang maintained community isolation and inter-city mobility control during the COVID-19 epidemic outbreak. On February 7, 2020, the medical resource aid to Hubei province was initiated by the joint prevention and control mechanism of the State Council. After February 11, 2020, the medical resource aid from other provinces gradually entered to Hubei province territory. Therefore, the numbers of hospital beds in the three cities before February 11, 2020, were considered as the initial medical resources, while the numbers of additional hospital beds in the three cities after February 11, 2020, were considered as the external medical resource aid during the COVID-19 outbreak. In scenario 7, medical resource aid was not implemented on February 11, 2020, while the numbers of hospital beds in the three cities remained at the initial medical resource levels. In scenario 8, medical resource aid was implemented 7 days later, while the numbers of hospital beds in the three cities remained at the initial medical resource levels until February 18, 2020, and were controlled and thus gradually increased after February 18, 2020. In scenario 9, medical resource aid was implemented 7 days earlier, while the numbers of hospital beds in the three cities started to increase on February 4, 2020.

4.5. Impact of intra-city movement on the COVID-19 spread

Fig. 7 illustrates the outcomes of the simulated epidemic spread in scenario 1 compared with the real epidemic spread in the three cities. The numbers of infected in the three cities increased sharply when the community isolation measures were lacking. The peak numbers of simulated infected in Wuhan was 129% larger than the real peak numbers of infected. The peak numbers of simulated infected in Jingzhou and Xiangyang were four times more than the real peak numbers of infected. The total numbers of simulated infected in Wuhan was 96% more than the real total numbers of infected. The total numbers of simulated infected in Jingzhou was 368% more than the real total numbers of infected. The total number of simulated infected in Xiangyang was 495% more than the real total numbers of infected. This outcome indicates that the lack of community isolation would significantly prolong the epidemic spread in all three cities. Thus, we can infer that the level I response, which restricts intra-city movements, has a significant effect on epidemic control.

Fig. 8 shows the outcomes of the simulated epidemic spread in scenario 2 compared with the real epidemic spread in the three cities. The number of infected in the three cities would significantly increase in the case of delayed implementation of community control measures. The peak number of simulated infected in Wuhan was 73% more than the real peak numbers of infected. The peak numbers of simulated infected in Jingzhou and Xiangyang were three times more than the real numbers of infected. The total number of simulated infected in Wuhan was 52% more than the real total numbers of infected. The total number of simulated infected in Jingzhou was 273% more than the real total numbers of infected. The total number of simulated infected in Xiangyang was 369% more than the real total numbers of infected. At the same time, the epidemic duration would be prolonged if community isolation measures were implemented 7 days late. Thus, we can infer that increasing intra-city population movements have positive effects on

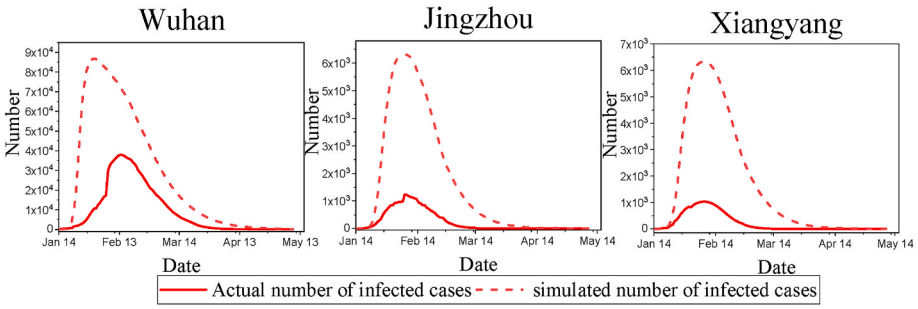

Fig. 7. Simulated spread by the SEIR-FMi model in scenario 1 compared with the real epidemic spread.

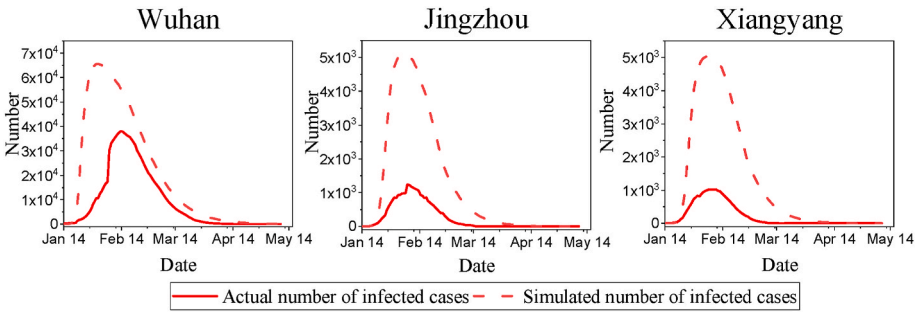

Fig. 8. Simulated spread by the SEIR-FMi model in scenario 2 compared with the real epidemic spread.

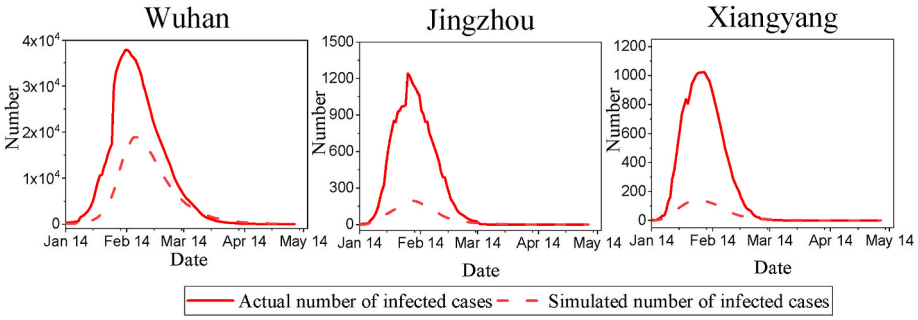

Fig. 9. Simulated spread by the SEIR-FMi model in scenario 3 compared with the real epidemic spread.

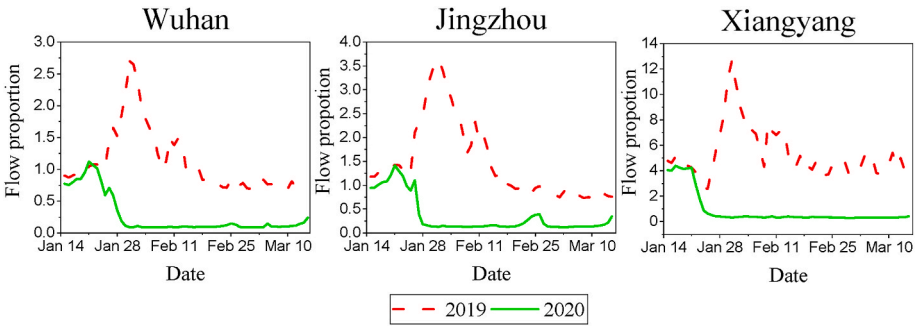

Fig. 10. Comparison of the proportions of population flow between 2019 and 2020 in Wuhan, Jingzhou, and Xiangyang from January 15 to March 15, 2020, and the same period in 2019 (according to the lunar calendar).

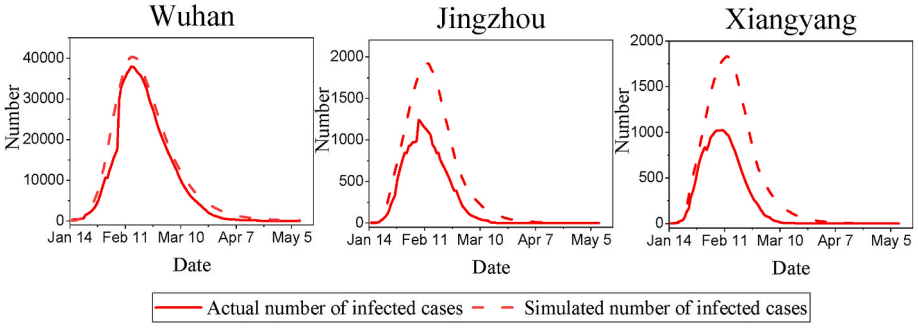

Fig. 11. Simulated spread by the SEIR-FMi model in scenario 4 compared with the real epidemic spread.

the spread of the epidemic.

Fig. 9 shows the outcomes of the simulated epidemic spread in scenario 3 compared with the real epidemic spread in the three cities. We see that the numbers of infected in the three cities would significantly decrease in the case of early implementation of community control measures. The peak number of simulated infected in Wuhan was 29% smaller than the real peak numbers of infected. The peak numbers of simulated infected in Jingzhou and Xiangyang were nearly 70% smaller than the real peak numbers of infected. The total number of simulated infected in Wuhan was 22% smaller than the real total numbers of infected. The total numbers of simulated infected in Jingzhou was 60% smaller than the real total number of infected. The total number of

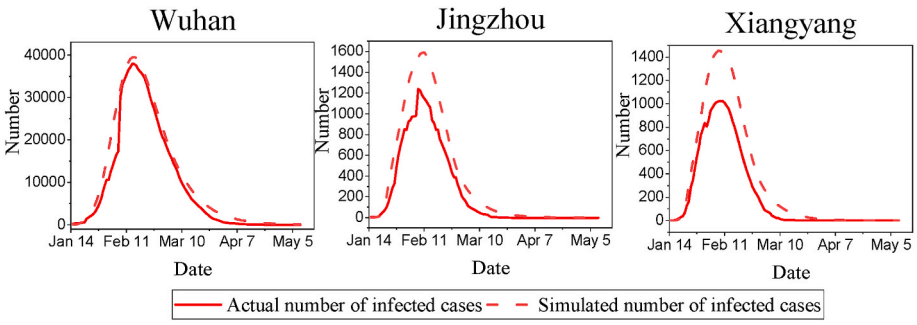

Fig. 12. Simulated spread by the SEIR-FMi model in scenario 5 compared with the real epidemic spread.

simulated infected in Xiangyang was 68% smaller than the real total number of infected. At the same time, the epidemic duration would be shortened in Jingzhou and Xiangyang if community isolation measures were implemented 7 days early. Thus, we can infer that decreasing intra-city population movements have negative effects on the spread of the epidemic.

4.6. Impact of inter-city movement on COVID-19

We used the population mobility data of the same period in 2019 and 2020 to study the impact of inter-city population movement on the spread of COVID-19 under the scenarios 4 to 6. Fig. 10 shows a comparison of the proportions of population flow among the three cities for the same period in 2019 and 2020. After the implementation of the level I response, the numbers of people moving into and moving out from the three cities in 2020 were significantly smaller than those in 2019.

Fig. 11 shows a comparison between the real epidemic spread and the model simulation results in scenario 4. The results show that if inter-city mobility control measures were not implemented during the Spring Festival in 2020, the numbers of infected in all the three cities would increase. The peak number of simulated infected in Wuhan was 6% more than the real peak numbers of infected. The peak numbers of simulated infected in Jingzhou and Xiangyang were more than the real peak numbers of infected by more than 50%. The total number of simulated infected in Wuhan was 7% more than the real total numbers of infected. The total numbers of simulated infected in Jingzhou was 81% more than the real total numbers of infected. The total number of simulated infected in Xiangyang was 105% more than the real total numbers of infected. At the same time, the duration of the epidemic would be prolonged in Jingzhou and Xiangyang if community isolation measures were not implemented. Thus, we can infer that the level I response, which increases inter-city population movements, will accelerate the spread of the epidemic and that the inter-city mobility control measure has a significant effect on epidemic control.

Fig. 12 shows the outcomes of the simulated spread in scenario 5 compared with the real epidemic spread in the three cities. The numbers of infected in the three cities would increase in the case of delayed implementation of inter-city mobility control measures. The peak number of simulated infected in Wuhan was 4% more than the real peak numbers of infected. The peak numbers of simulated infected in Jingzhou and Xiangyang were more than the real peak numbers of infected by more than 25%. The total numbers of simulated infected in Wuhan was 5% more than the real total numbers of infected. The total number of simulated infected in Jingzhou was 40% more than the real total numbers of infected. The total number of simulated infected in Xiangyang was 46% more than the real total numbers of infected. Meanwhile, the duration of the epidemic would be prolonged if inter-city mobility control measures were implemented 7 days later.

Fig. 13 shows a comparison between the real epidemic spread and the model simulation results in scenario 6. The numbers of infected in the city of Jingzhou and Xiangyang would decrease if inter-city mobility control measures were implemented 7 days early, but the number of infected did not change significantly in Wuhan. The peak numbers of simulated infected in Jingzhou and Xiangyang were nearly 40% smaller than the real peak numbers of infected. The total number of simulated infected in Jingzhou was 25% smaller than the real total number of infected. The total number of simulated infected in Xiangyang was 31% smaller than the real total numbers of infected. Thus, we can infer that restricted inter-city population movements affect epidemic control. However, different cities have different impact levels, with low-risk cities being affected more than high-risk cities.

4.7. Impact of medical resource investment on the spread of COVID-19

Fig. 14 shows a comparison between the real epidemic spread and the model simulation results in scenario 7. The number of simulated infected remains approximately the same as the real number of infected at the beginning of the epidemic spread. After February 11, 2020, the numbers of infected in the three cities in the real situation peaked, and the growth rate in the number of cured cases gradually increased. This is because the increasing number of medical resources invested in Hubei province led to a significant acceleration in the recovery rate after February 11. Meanwhile, an increase in the number of recoveries would also reduce the number of new infections and play a preventive role in

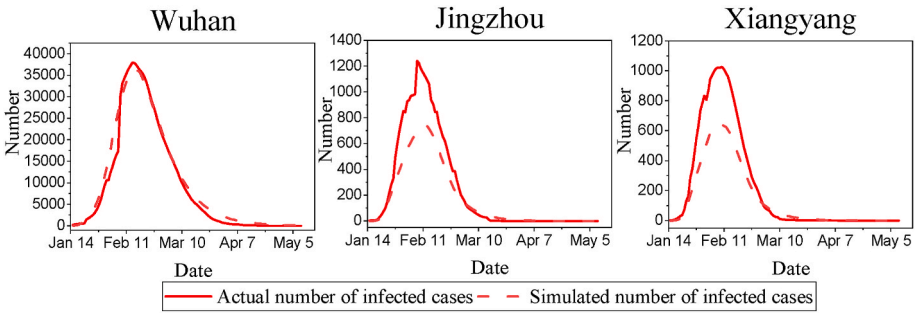

Fig. 13. Simulated spread by the SEIR-FMi model in scenario 6 compared with the real epidemic spread.

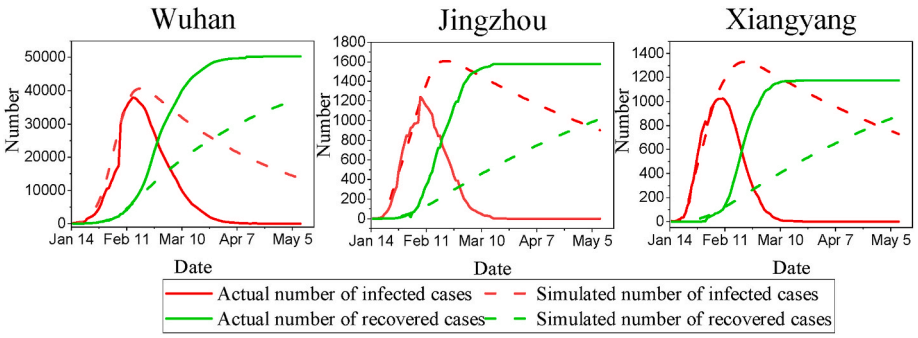

Fig. 14. Simulated spread by the SEIR-FMi model under scenario 7 compared with the real epidemic spread.

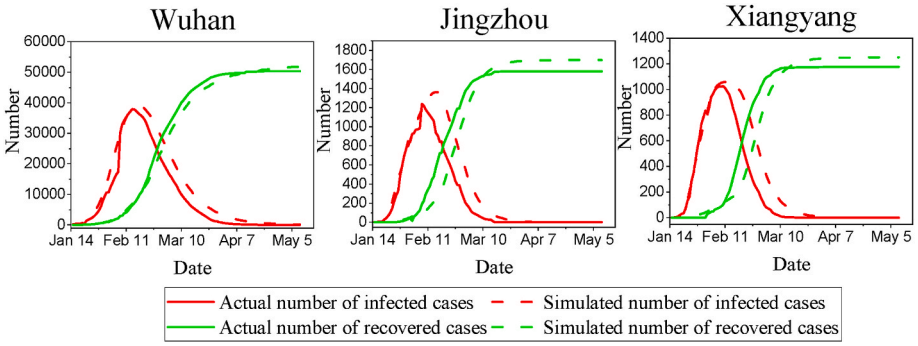

Fig. 15. Simulated spread by the SEIR-FMi model in scenario 8 compared with the real epidemic spread.

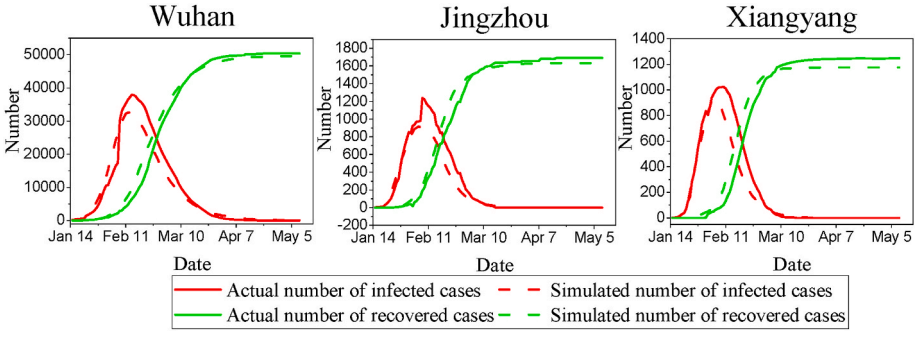

Fig. 16. Simulated spread by the SEIR-FMi model in scenario 9 compared with the real epidemic spread.

the epidemic outbreak. Nevertheless, the simulation results also indicate that the number of infected cases after February 11 remained at the same growth rate as before and would not reach its peak immediately. The reason here is that without the investment of external medical resources, more and more infected cases would not be treated timely and recovered. Then, the infected cases would infect more susceptible individuals in real practice. For example, during the early stage of the COVID-19 outbreak in Wuhan in 2020, some infected cases had to be quarantined at home due to the shortage of hospital beds, and this cause many of their family members infected as they cannot isolate themselves completely in their daily life.

Fig. 15 shows the outcomes of the simulated spread in scenario 8 compared with the real epidemic spread in the three cities. As shown in Fig. 15, the numbers of infected cases in all three cities would increase after February 11 if medical resource investment measures were implemented 7 days late. The total number of simulated infected in Wuhan was 2% more than the real total numbers of infected. The total number of simulated infected in Jingzhou was 13% more than the real total numbers of infected. The total number of simulated infected in Xiangyang was 16% more than the real total numbers of infected. The epidemic duration would be prolonged if the medical resource aid measure was implemented 7 days late. At the same time, the simulated number of recoveries was smaller than the real number of recoveries between February 13 and March 1 because the delay in medical resource investment led to a decrease in recovery rate. At the late stage of the epidemic, medical resources were increased, and the recovery rate in the simulation was improved. However, as the number of infected cases in the early stage increased, the number of recoveries by the model simulation was more than the real number.

Fig. 16 shows the outcomes of the simulated spread in scenario 9 compared with the real epidemic spread in the three cities. Between February 9 and March 1, the numbers of simulated infected in all three cities were smaller than the numbers of real infected cases, but the number of simulated recoveries were more than the real number of recoveries. Meanwhile, the recovery rate by the simulation model was higher than the real recovery rate, as the early implementation of medical resource aid measure. At the late stage of the epidemic, the number of simulated recovered is smaller than the real number because of the decrease in the number of infected cases in the early stages.

Table 7
Comparison between the simulated total number of infections and the real total number of infections under different scenarios.

Response	Scenario	Indicator	Wuhan	Jingzhou	Xiangyang
Intra-city population movement	1	number of infected cases	+96%	+368%	+495%
		peak number	+129%	+409%	+517%
	2	number of infected cases	+52%	+273%	+369%
		peak number	+73%	+310%	+392%
	3	number of infected cases	−22%	−60%	−68%
		peak number	−29%	−70%	−73%
Inter-city population movement	4	number of infected cases	+7%	+81%	+105%
		peak number	+6%	+55%	+79%
	5	number of infected cases	+5%	+40%	+46%
		peak number	+4%	+28%	+42%
	6	number of infected cases	−1%	−25%	−31%
		peak number	−3%	−40%	−37%
Medical resource investment	7	number of infected cases	+1%	+44%	+45%
		peak number	+3%	+49%	+41%
	8	number of infected cases	+2%	13%	+16%
		peak number	+3%	10%	+13%
	9	number of infected cases	−2%	−19%	−20%
		peak number	−3%	−22%	−19%

4.8. Summary of simulation results

Table 7 shows the outcomes of the total and peak numbers of infected cases derived from the simulation compared with the real number of infected cases in the three cities. Here, the values represent the percentage difference between the real and simulated results. The positive value indicates that the simulated number is larger than the real number, and the negative value indicates that the simulated number is smaller than the real number. Scenarios 1 to 3 reflect the impact of the intra-city population movement on the spread of COVID-19. Scenarios 4 to 6 reflect the impact of inter-city population movement on the spread of COVID-19. Scenarios 7 to 9 reflect the impact of medical resources on the spread of COVID-19.

On the basis of the simulation results, we can infer that first, the impact levels of the three factors on the number of infections is as follows: intra-city population movement > inter-city population movement > medical resource investment. This indicates that during the epidemic outbreak in the cities, controlling the movements of people within cities by, for example, implementing community isolation, restricting gatherings, and closing public places plays the most important role in the prevention and control of epidemic. This result also shows that controlling crowd contact is the most fundamental preventive approach against the spread of infectious diseases.

Second, either to delay or implement community control measure, the impact of intra-city movement on the spread of COVID-19 will be much greater in the low-risk areas such as Jingzhou and Xiangyang than that in the high-risk areas such as Wuhan. This result is mainly due to two reasons. On the one hand, a few days before the level I response was implemented, the intra-city movement intensity in Wuhan had already started to decline and was at a lower state because a COVID-19 outbreak had already started in Wuhan. However, owing to the Spring Festival, the intra-city movement intensities in Jingzhou and Xiangyang were in the increasing stage and at their peaks on the January 24th. Therefore, the change in intra-city movement intensity caused by the early or delayed implementation of emergency response measures was more pronounced for Jingzhou and Xiangyang than for Wuhan. On the other hand, as depicted in Fig. 3, before the level I response was implemented, a large flow of people from the high-risk city (Wuhan) to the low-risk cities (Jingzhou and Xiangyang) due to the COVID-19 epidemic outbreak and Spring Festival was observed. This would cause a larger number of potential contagions from high-to low-risk cities and increase the threat of the epidemic in low-risk areas.

Third, regardless of whether inter-city mobility control measures were delayed or implemented, inter-city population movement had a relatively small impact on the epidemic spread in Wuhan as a high-risk city but a large impact on the epidemic spread in Jingzhou and Xiangyang as low-risk cities. This is because the high-risk cities export a higher proportion of potentially infected individuals, so they have a greater impact on low-risk cities. On the contrary, a smaller proportion of potentially infected individuals are exported from low-risk cities, so it has a smaller impact on high-risk cities. In addition, high-risk areas, where the epidemic is worse, are usually prioritized in the implementation of social distancing and medical resource investments. However, from to our simulation results, we found that increasing the intensity of control and medical resource investment in low-risk areas will bring more significant effects.

4.9. Sensitivity analysis experiments

In this section, based on the collected data in Section 4.1, we conduct a series of sensitivity analysis on the parameters as different sizes and risk levels of the cities to investigate the robustness of experimental outcomes.

First, we define two types of cities based on city size, namely large and small city. The large city has more population (including resident population and migrant population) as well as larger number of initial hospital beds than small city. We assume that the large city has the similar population, initial hospital beds and intra-city movement intensity as that of Wuhan, and that the small city has the similar population, initial hospital beds and intra-city movement intensity as that of Jingzhou. The proportion of migrant population between large city and small city is similarly to that between Wuhan and Jingzhou. The proportion of migrant movement population between two cities of equal size is similarly to that between Jingzhou and Xiangyang.

Second, we define two types of risk levels of the cities, namely high-

Table 8
Sensitivity analysis experiments scenarios design.

Scenario	City A	City B	City C
10	Large city with low risk level	Small city with high risk level	Small city with low risk level
11	Large city with low risk level	Small city with low risk level	Small city with low risk level
12	Large city with high risk level	Large city with low risk level	Large city with low risk level
13	Large city with low risk level	Large city with high risk level	Small city with low risk level
14	Large city with low risk level	Large city with low risk level	Small city with high risk level

Table 9
The results in peak numbers and total number of infected with and without control measures in sensitivity analysis.

Scenario	Response	Indicator	City A	City B	City C
10	Intra-city population movement	peak number	+482%	+54%	+423%
		number of infected cases	+500%	+48%	+406%
	Inter-city population movement	peak number	+208%	+23%	+96%
		number of infected cases	+201%	+38%	+96%
	Medical resource investment	peak number	+26%	+6%	+18%
		number of infected cases	+26%	+9%	+16%
11	Intra-city population movement	peak number	+212%	+114%	+114%
		number of infected cases	+242%	+169%	+169%
	Inter-city population movement	peak number	+12%	+35%	+35%
		number of infected cases	+15%	+38%	+38%
	Medical resource investment	peak number	+6%	+9%	+9%
		number of infected cases	+7%	+14%	+14%
12	Intra-city population movement	peak number	+60%	+314%	+314%
		number of infected cases	+46%	+300%	+301%
	Inter-city population movement	peak number	+15%	+124%	+124%
		number of infected cases	+11%	+117%	+117%
	Medical resource investment	peak number	+36%	+47%	+47%
		number of infected cases	+30%	+67%	+67%
13	Intra-city population movement	peak number	+512%	+61%	+332%
		number of infected cases	+355%	+53%	+308%
	Inter-city population movement	peak number	+45%	+8%	+312%
		number of infected cases	+36%	+8%	+321%
	Medical resource investment	peak number	+15%	+10%	+15%
		number of infected cases	+16%	+9%	+16%
14	Intra-city population movement	peak number	+271%	+271%	+66%
		number of infected cases	+407%	+407%	+59%
	Inter-city population movement	peak number	+93%	+93%	+22%
		number of infected cases	+98%	+98%	+36%
	Medical resource investment	peak number	+8%	+8%	+6%
		number of infected cases	+5%	+5%	+10%

risk city and low-risk city. The high-risk city means that the city is the source city of the epidemic and has more initial number of infected cases than the low-risk city. We assume that the high-risk city has the similar proportion of initial number of infected cases and population as that of Wuhan, and the low-risk city has the similar proportion of initial number of infected cases and population as that of Jingzhou. For high-risk city, the effective infection rate and, the number and speed of the increase in hospital beds is similar to that of Wuhan. For low-risk city, it has the similar situation as that of Jingzhou.

Based on the different sizes and risk levels of cities, we design five simulation scenarios in Table 8. In scenario 10 to 14, we assume that all the three cities, namely city A, city B and city C, implement control measures, i.e., with level I public health emergency response on January 24, 2020 to control intra-city and inter-city population movement and invest medical resource. In the appendix, we present the simulated epidemic trends for each scenario.

In each scenario, we compare the differences in peak numbers and total numbers of infected cases with and without population movement control measures (including intra-city movement and inter-city movement) and medical resource investments measures. Table 9 shows the percentage increase in the total number and in the peak number of infected cases with the absence of control measures. We can see that in all the scenarios, the percentage increase with intra-city population movement is larger than that with inter-city population movement, and the percentage increase with intra-city population movement is larger than that with medical resource investment. Without the control on inter-city population movement, the low-risk city have larger percentage increases in peak numbers and total numbers of infected cases than those of the high-risk city. This indicates that the experimental results on the rank of impacts of the three measures on the number of infections is robust. The control measures such as community isolation and social distance exert the most important role to prevent the epidemic outbreak. With population movement restriction, it is more effective to prevent the spread of COVID-19 in low-risk cities than in high-risk cities. The epidemic trends in the sensitivity analysis are shown in the appendix.

5. Discussion

The above simulation experiments of the COVID-19 epidemic illustrates that the level I public health emergency response, including community isolation, population mobility control, and medical resource investment, implemented in early 2020 in Hubei province significantly reduced the contact probability between the susceptible and infected populations and reduced the risk of epidemic transmission. Meanwhile, the implemented response accelerated the treatment of patients with COVID-19 and shortened the epidemic development period. From the experimental results, we can make the following three advices to control the spread of the COVID-19 epidemic worldwide.

First, we should reduce the intra-city movement and increase personal protection. Reducing the intensity of contact between people is an effective measure to control the spread of the epidemic. Therefore, during the large-scale epidemic outbreak, intra-city population movements should be controlled to avoid the gathering of people. Meanwhile, personal protection should be applied to reduce direct human-to-human contact by wearing masks and keeping social distance. Public places should be ventilated in a timely manner to reduce the probability of people being infected with the virus.

Second, we should control population movement and reduce population access to high-risk areas. During the epidemic, the population mobility between cities should be controlled, especially in high-risk areas. On the one hand, the inflow of people should be controlled to avoid importing infected cases. On the other hand, the outflow of people should be monitored to reduce the risk of infection of susceptible people in other cities during their travel.

Third, the medical and quarantine supply aids, inoculation rates, and the scope of vaccination should be augmented. During the epidemic, it is important to speed up treatment of infected patients by increasing medical investments and screening of exposed populations by increasing quarantine supplies. Meanwhile, it is also an effective measure to combat infectious diseases by increasing the number of immune persons through widespread vaccinations.

6. Conclusion

Since the late December of 2019, the COVID-19 epidemic has rapidly spread in Wuhan and gradually spread to many countries and regions worldwide, causing millions of victims. To study the spread of the COVID-19 epidemic, many epidemiological models have been proposed to predict the number of infected people, estimate the development of COVID-19, and assess the prevention and control measures. However, in most existing models, the effects of population mobility in different cities and medical resource assistance from other provinces on the spread of COVID-19 are ignored. In this paper, first, we propose a novel epidemiological model called SEIR-FMi that considers three factors, namely intra-city population movement, inter-city population movement, and medical resource investment. We theoretically derived the basic reproduction number and effective reproduction number of the proposed SEIR-FMi model and analyzed the effects of the three factors on the development of the COVID-19 epidemic. Second, we used the

proposed SEIR-FMi model to simulate the spread of COVID-19 to account for the effect of the level I public health emergency response, which includes community isolation, population mobility control, and outside medical resource assistance, on the epidemic spread in Hubei province between January 15, 2020, and May 20, 2020. The simulation results show that the SEIR-FMi model is good at fitting the COVID-19 epidemic in the cities of Wuhan, Jingzhou, and Xiangyang in this period.

According to the simulation results in this study, first, the intra-city population movement can accelerate the spread of COVID-19. High-intensity intra-city population movement would cause a high contact probability between susceptible and infected populations, which would in turn increase the infection risk of the susceptible population. Second, the population mobility among cities with different risk levels has different affects the epidemic spread. In high-risk cities, an increase in inter-city population movement will reduce the number of infected individuals in the city and mitigate the development of the epidemic. However, the influx of large numbers of exposed individuals from the high-risk cities would significantly increase the number of infected people in the low-risk cities. Meanwhile, the mobile population can also lead to an increase in the total number of infected people in all cities because the exposed population in the movement population have a higher risk of contact with susceptible people. Finally, the medical resource investment would impact the epidemic spread in two ways. First, medical resource aid would reduce the growth rate of the number of infected individuals and reduce the peak number of COVID-19 infections. Second, medical resource aid would speed up the recovery of infected patients and reduce the development period of the epidemic. Thus, more medical resource investments could effectively reduce the total number of infected individuals in the COVID-19 epidemic, which positively affects the prevention and control of the epidemic.

Acknowledgments

This research is supported in part by National Natural Science Foundation of China under Grant Nos. 72174018, 71932002 and 72071005; the Beijing Youth Talent Fund under Grant No. Q0011019202001; the Beijing Natural Science Foundation under Grant No. 9222001; the Philosophy and Sociology Science Fund from Beijing Municipal Education Commission (SZ202110005001); the Beijing Nova Program of Science & Technology under Grant No. Z191100001119100. Research of Prof. Santibanez-Gonzalez was partially funded by FONDECYT Grant No. 1190559.

Appendix A. Supplementary data

Supplementary data to this article can be found online at https://doi.org/10.1016/j.compbiomed.2022.106046.

References

[1] X. Tian, et al., Potent binding of 2019 novel coronavirus spike protein by a SARS coronavirus-specific human monoclonal antibody, Emerg. Microb. Infect. 9 (1) (2020) 382–385, https://doi.org/10.1080/22221751.2020.1729069.
[2] S. Chang, et al., Mobility network models of COVID-19 explain inequities and inform reopening, Nature (2020), https://doi.org/10.1038/s41586-020-2923-3.
[3] J.T. Wu, K. Leung, G.M. Leung, Nowcasting and forecasting the potential domestic and international spread of the 2019-nCoV outbreak originating in Wuhan, China: a modelling study, Lancet 395 (10225) (2020) 689–697, https://doi.org/10.1016/S0140-6736(20)30260-9.
[4] I. Cooper, A. Mondal, C.G. Antonopoulos, A SIR model assumption for the spread of COVID-19 in different communities, Chaos, Solit. Fractals 139 (2020), 110057, https://doi.org/10.1016/j.chaos.2020.110057.
[5] N. Piovella, Analytical solution of SEIR model describing the free spread of the COVID-19 pandemic, Chaos, Solit. Fractals 140 (2020), 110243, https://doi.org/10.1016/j.chaos.2020.110243.
[6] Z. Yang, et al., Modified SEIR and AI prediction of the epidemics trend of COVID-19 in China under public health interventions, J. Thorac. Dis. 12 (3) (2020) 165–174, https://doi.org/10.21037/jtd.2020.02.64.
[7] R. Mu, A. Wei, Y. Yang, Global dynamics and sliding motion in A(H7N9)epidemic models with limited resources and Filippov control, J. Math. Anal. Appl. 477 (2) (2019) 1296–1317, https://doi.org/10.1016/j.jmaa.2019.05.013.
[8] M. Chen, M. Li, Y. Hao, Z. Liu, L. Hu, L. Wang, The introduction of population migration to SEIAR for COVID-19 epidemic modeling with an efficient intervention strategy, Inf. Fusion 64 (August) (2020) 252–258, https://doi.org/10.1016/j.inffus.2020.08.002.
[9] J.E. Cohen, Infectious diseases of humans: dynamics and control, JAMA, J. Am. Med. Assoc. 6 (10) (1991) 340–341, https://doi.org/10.1016/0169-5347(91)90048-3.
[10] N.C. Grassly, C. Fraser, Mathematical models of infectious disease transmission, Nat. Rev. Microbiol. 6 (6) (2008) 477–487, https://doi.org/10.1038/nrmicro1845.
[11] S.H. White, A.M. del Rey, G.R. Sánchez, Modeling epidemics using cellular automata, Appl. Math. Comput. 186 (1) (2007) 193–202, https://doi.org/10.1016/j.amc.2006.06.126.
[12] A. Bouaine, M. Rachik, Modeling the impact of immigration and climatic conditions on the epidemic spreading based on cellular automata approach, Ecol. Inf. 46 (2018) 36–44, https://doi.org/10.1016/j.ecoinf.2018.05.004. September 2017.
[13] P.C.L. Silva, P.V.C. Batista, H.S. Lima, M.A. Alves, F.G. Guimarães, R.C.P. Silva, COVID-ABS: an agent-based model of COVID-19 epidemic to simulate health and economic effects of social distancing interventions, Chaos, Solit. Fractals 139 (2020), https://doi.org/10.1016/j.chaos.2020.110088.
[14] O.M. Cliff, N. Harding, M. Piraveenan, E.Y. Erten, M. Gambhir, M. Prokopenko, Investigating spatiotemporal dynamics and synchrony of influenza epidemics in Australia: an agent-based modelling approach, Simulat. Model. Pract. Theor. 87 (2018) 412–431, https://doi.org/10.1016/j.simpat.2018.07.005.
[15] Y. Wei, J. Wang, W. Song, C. Xiu, L. Ma, T. Pei, Spread of COVID-19 in China: analysis from a city-based epidemic and mobility model, October, Cities (2020), 103010, https://doi.org/10.1016/j.cities.2020.103010.
[16] G.C. Sirakoulis, I. Karafyllidis, A. Thanailakis, A cellular automaton model for the effects of population movement and vaccination on epidemic propagation, Ecol. Model. 133 (3) (2000) 209–223, https://doi.org/10.1016/S0304-3800(00)00294-5.
[17] R.M. May, A.L. Lloyd, Infection dynamics on scale-free networks, Phys. Rev. E 64 (6) (2001) 4, https://doi.org/10.1103/PhysRevE.64.066112.
[18] R. Pastor-Satorras, C. Castellano, P. Van Mieghem, A. Vespignani, Epidemic processes in complex networks, Rev. Mod. Phys. 87 (3) (2015), https://doi.org/10.1103/RevModPhys.87.925.
[19] C. Moore, M.E.J. Newman, Epidemics and percolation in small-world networks, Phys. Rev. E 61 (5) (2000) 5678–5682, https://doi.org/10.1103/PhysRevE.61.5678.
[20] M. Boots, A. Sasaki, 'Small worlds' and the evolution of virulence: infection occurs locally and at a distance, Proc. R. Soc. B Biol. Sci. 266 (1432) (1999) 1933–1938, https://doi.org/10.1098/rspb.1999.0869.
[21] M.E.J. Newman, Spread of epidemic disease on networks, Phys. Rev. E 66 (1) (2002) 1–11, https://doi.org/10.1103/PhysRevE.66.016128.
[22] M.J. Keeling, K.T.D. Eames, Networks and epidemic models, J. R. Soc. Interface 2 (4) (2005) 295–307, https://doi.org/10.1098/rsif.2005.0051.
[23] M.A.G. Kermack W O, A contribution to the mathematical theory of epidemics, Proc. R. Soc. London. Ser. A, Contain. Pap. a Math. Phys. Character 115 (772) (1927) 700–721, https://doi.org/10.1098/rspa.1927.0118.
[24] B. Tang, et al., Estimation of the transmission risk of the 2019-nCoV and its implication for public health interventions, J. Clin. Med. 9 (2) (2020) 462, https://doi.org/10.3390/jcm9020462.
[25] C. Castillo-Chavez, C.W. Castillo-Garsow, A.A. Yakubu, Mathematical models of isolation and quarantine, JAMA, J. Am. Med. Assoc. 290 (21) (2003) 2876–2877, https://doi.org/10.1001/jama.290.21.2876.
[26] E. Shim, Z. Feng, M. Martcheva, C. Castillo-Chavez, An age-structured epidemic model of rotavirus with vaccination, J. Math. Biol. 53 (4) (2006) 719–746, https://doi.org/10.1007/s00285-006-0023-0.
[27] X. Duan, S. Yuan, X. Li, Global stability of an SVIR model with age of vaccination, Appl. Math. Comput. 226 (2014) 528–540, https://doi.org/10.1016/j.amc.2013.10.073.
[28] W. Wang, G. Mulone, Threshold of disease transmission in a patch environment, J. Math. Anal. Appl. 285 (1) (2003) 321–335, https://doi.org/10.1016/S0022-247X(03)00428-1.
[29] S. Ruan, W. Wang, S.A. Levin, The effect of global travel on the spread of SARS, Math. Biosci. Eng. 3 (1) (2006) 205–218, https://doi.org/10.3934/mbe.2006.3.205.
[30] C. Hou, et al., The effectiveness of quarantine of Wuhan city against the Corona Virus Disease 2019 (COVID-19): a well-mixed SEIR model analysis, J. Med. Virol. 92 (7) (2020) 841–848, https://doi.org/10.1002/jmv.25827.
[31] T. Zhou, et al., Preliminary prediction of the basic reproduction number of the Wuhan novel coronavirus 2019-nCoV, J. Evid. Base Med. 13 (1) (2020) 3–7, https://doi.org/10.1111/jebm.12376.
[32] M.Y. Li, J.S. Muldowney, Global stability for the SEIR model in epidemiology, Math. Biosci. 125 (2) (1995) 155–164, https://doi.org/10.1016/0025-5564(95)92756-5.
[33] M.H.A. Biswas, L.T. Paiva, M. De Pinho, A seir model for control of infectious diseases with constraints, Math. Biosci. Eng. 11 (4) (2014) 761–784, https://doi.org/10.3934/mbe.2014.11.761.
[34] M.C. González, C.A. Hidalgo, A.L. Barabási, Understanding individual human mobility patterns, Nature 453 (7196) (2008) 779–782, https://doi.org/10.1038/nature06958.
[35] I. Hanski, Metapopulation theory, its use and misuse, Basic Appl. Ecol. 5 (3) (2004) 225–229, https://doi.org/10.1016/j.baae.2004.03.002.

[36] M. Gatto, et al., Spread and dynamics of the COVID-19 epidemic in Italy: effects of emergency containment measures, Proc. Natl. Acad. Sci. U.S.A. 117 (19) (2020) 10484–10491, https://doi.org/10.1073/pnas.2004978117.
[37] S. Lai, et al., Effect of non-pharmaceutical interventions to contain COVID-19 in China, Nature (2020), https://doi.org/10.1038/s41586-020-2293-x.
[38] C. Shan, H. Zhu, Bifurcations and complex dynamics of an SIR model with the impact of the number of hospital beds, J. Differ. Equ. 257 (5) (2014) 1662–1688, https://doi.org/10.1016/j.jde.2014.05.030.
[39] W. Wang, Backward bifurcation of an epidemic model with treatment, Math. Biosci. 201 (1–2) (2006) 58–71, https://doi.org/10.1016/j.mbs.2005.12.022.
[40] X. Zhang, X. Liu, Backward bifurcation of an epidemic model with saturated treatment function, J. Math. Anal. Appl. (2008), https://doi.org/10.1016/j.jmaa.2008.07.042.
[41] G.H. Li, Y.X. Zhang, Dynamic behaviors of a modified SIR model in epidemic diseases using nonlinear incidence and recovery rates, PLoS One 12 (4) (2017) 1–28, https://doi.org/10.1371/journal.pone.0175789.
[42] P. Van Den Driessche, J. Watmough, Reproduction numbers and sub-threshold endemic equilibria for compartmental models of disease transmission, Math. Biosci. 180 (1–2) (2002) 29–48, https://doi.org/10.1016/S0025-5564(02)00108-6.
[43] M. Raghavan, K.S. Sridharan, Y. Mandayam Rangayyan, Using epidemic simulators for monitoring an ongoing epidemic, Sci. Rep. (2020), https://doi.org/10.1038/s41598-020-73308-5.
[44] S. Wei, L. Wang, Examining the population fl ow network in China and its implications for epidemic control based on Baidu migration data, Humanit. Soc. Sci. Commun. 7 (1) (2020) 1–10, https://doi.org/10.1057/s41599-020-00633-5.
[45] C. Zhou, F. Su, T. Pei, A. Zhang, Y. Du, B. Luo, Geography and sustainability COVID-19 : challenges to GIS with big data, Geogr. Sustain. J. 1 (2020) 77–87, https://doi.org/10.1016/j.geosus.2020.03.005.
[46] J. Zu, M.L. Li, Z.F. Li, M.W. Shen, Y.N. Xiao, F.P. Ji, Transmission patterns of COVID-19 in the mainland of China and the efficacy of different control strategies: a data- and model-driven study, Infect. Dis. Poverty 9 (1) (2020) 1–14, https://doi.org/10.1186/s40249-020-00709-z.
[47] U. Avila-Ponce de León, Á.G.C. Pérez, E. Avila-Vales, An SEIARD epidemic model for COVID-19 in Mexico: mathematical analysis and state-level forecast, Chaos, Solit. Fractals 140 (2020), https://doi.org/10.1016/j.chaos.2020.110165.
[48] S. Cauchemez, F. Carrat, C. Viboud, A.J. Valleron, A Bayesian MCMC approach to study transmission of in uenza : application to household longitudinal data, Stat. Med. 23 (2004) 3469–3487, https://doi.org/10.1002/sim.1912.
[49] J. Ge, D. He, Z. Lin, H. Zhu, Z. Zhuang, Four-tier response system and spatial propagation of COVID-19 in China by a network model, Math. Biosci. 330 (2020), https://doi.org/10.1016/j.mbs.2020.108484 no. October, p. 108484.